MANY-QUANTUM TRANSITIONS IN THE CONDUCTION
ELECTRON SPIN SYSTEM OF LITHIUM METAL

by

TERRY KOSS

B.Sc., University of Washington,
1966

A THESIS SUBMITTED IN PARTIAL FULFILMENT OF

THE REQUIREMENTS FOR THE DEGREE OF

MASTER OF SCIENCE

in the department of

PHYSICS

We accept this thesis as conforming to the required standard.

THE UNIVERSITY OF BRITISH COLUMBIA

July 1968

ABSTRACT

Resonance absorption spectra have been observed which may be interpreted as many-quantum transitions where the axis of quantization is along the effective magnetic field in the rotating frame. By this description, resonances which required up to five quanta were observed. The spin system used was that of conduction electrons of lithium metal in neutron irradiated lithium fluoride crystals. An analysis of the experimental results using a modified Bloch equation under the assumption that $\tau_1 = \tau_2 = \tau \approx 1.5 \times 10^{-7}$ sec. and that the spin system relaxes toward the instantaneous field is presented. A brief outline of the concept of spin temperature is included. A comparison is made between some of the predictions of the spin temperature concept and the simple Bloch theory used in analyzing the experimental data.

(iii)

TABLE OF CONTENTS

LIST OF FIGURES

LIST OF FIGURES (continued)

ACKNOWLEDGEMENT

1. INTRODUCTION

The classical equation describing the motion of a free
magnetic dipole with a dipole moment μ in a static magnetic
field H_0 is

$$\frac{d\bar{\mu}}{dt} = \bar{\mu} \times \gamma \bar{H}_0 \qquad (1.1)$$

where γ is defined by the relation $\mu = \gamma J$ and J is the angular
momentum of the dipole. γ is called the gyromagnetic ratio.
This equation is generally solved by noting that in a
coordinate system rotating at an angular frequency ω around
the axis which is parallel to H_0 the equation of motion of
the dipole moment becomes:

$$\frac{d\bar{\mu}}{dt} = \bar{\mu} \times (\gamma \bar{H}_0 + \omega) \qquad (1.2)$$

The magnetic moment is thus stationary in a frame rotating
at $\omega = -\gamma H_0$. This solution then is easily transformed back to
the laboratory frame. Likewise it is easy to show that in
the quantum theory the equation for the expection value of
the magnetic moment for an isolated spin is given by

$$\frac{d\langle\bar{\mu}\rangle}{dt} = \langle\bar{\mu}\rangle \times \gamma \bar{H}_0 \qquad (1.3)$$

which is just the classical equation. In addition if the
spins are non-interacting the expectation value of the total
magnetization obeys the same equation. The rotating reference
frame mentioned above assumes special importance when a rotating
magnetic field of frequency Ω and magnitude H_1 is applied
perpendicular to the static field H_0. In this case there
is a static field H_{eff} in the rotating frame and an analysis

similar to that above shows that the magnetization should

precess about H_{eff} viewed in the rotating frame. Thus it

is seen that the rotating frame is a useful device for

visualizing the resonance process. The angular frequency

of the precession of the spins in the rotating frame is given

$$H_{eff} = \left[\left(H_o - \frac{\omega}{\gamma} \right)^2 + H_1^2 \right]^{1/2}$$

(a) LAB FRAME

$H_z = H_o$
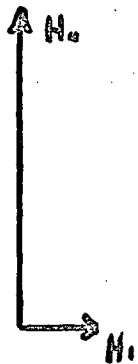
$H_x = H_1 \cos \omega t$

$H_y = H_1 \sin \omega t$
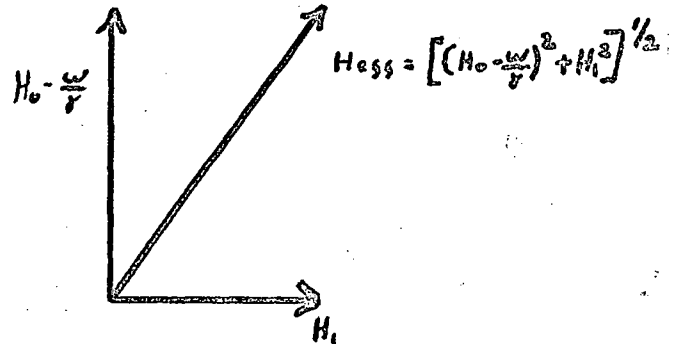
(b) ROTATING FRAME

$H_z = H_o - \frac{\omega}{\gamma}$

$H_x = H_1$

$H_y = 0$

FIGURE 1.

by $\omega eff = \gamma Heff$. Figure 1 shows the magnetic fields as viewed

in the lab frame and the rotating frame.

It is obvious from the above discussion that when $(H_o - \frac{\omega}{\gamma}) = 0$

the effective field is just H_1 and as the magnetization

precesses about this field its time average in the z direction

is zero. So far in the discussion all interactions of the

spins with the lattice or themselves has been neglected. In

real systems there are spin-lattice interactions which cause

the spin system to tend toward the thermal equilibrium value

it would have in the absence of a rotating field. There are thus two competing processes, the rotating field causing the magnetization to precess about H_{eff} and the spin lattice relaxation processes causing the magnetization to relax toward H_o. However even in the case of very strong spin-lattice coupling corresponding to characteristic relaxation times τ shorter than the spin Larmor precession period there should be, in the rotating frame, a net component of magnetization along H_{eff} given by the usual expression for the thermal equilibrium of the magnetization of a spin system in a static magnetic field.[1]

$$M_{eff} = N\mu_{eff}^2 \left(\beta^2 / 3kT \right) H_{eff} \qquad (1.4)$$

If on the other hand τ is comparable to or larger than the Larmor precession period the magnitude of the magnetization along H_{eff} can be much larger. This situation can be described by defining a new temperature T_{spin} such that equation 1.4 remains valid for the given magnetization. In any case it is possible to cause a resonance in the rotating frame by applying a perturbing field of the correct frequency perpendicular to H_{eff}.

Redfield[2] developed an essentially thermodynamic description of resonance experiments in the rotating frame. One of the assumptions of the theory as outlined in Miss Franz's thesis[3] is that the spin-spin interaction is large compared to the spin lattice interaction. This implies that the spin system can have a temperature different from that of the lattice. The

starting point for this theory is the assumption of a system

Hamiltonian of the form $H = H_z + H_{ss}$ where H_z is the Zeeman

interaction energy and H_{ss} is the spin-spin coupling energy.

Note that this Hamiltonian ignores any spin-lattice interaction.

The Hamiltonian is transformed to the rotating frame through

two transformation operators.

$$H^* = e^{i\omega I_z \tau} H e^{-i\omega I_z t} \qquad (1.5)$$

$$H^{*'} = e^{i\theta I_y} H^* e^{-i\theta I_y} \qquad (1.6)$$

The first takes the system into a frame rotating at angular

frequency ω around the z axis. The second aligns the axis

of quantization along the effective field axis. The resulting

Hamiltonian is:

$$\hbar H^{*'} = -\gamma \hbar H_{eff} I_z + \sum_{k>j} \left\{ A_{jk\rho} \overline{I}_j \cdot \overline{I}_k + \beta_{jk\rho} I_{jz} I_{kz} + D_{jk\rho} \left[I_{j+} I_{k+} + I_{j-} I_{k-} \right] \right.$$
$$\left. + E_{jk\rho} \left[(I_{j+} + I_{j-}) I_{kz} + I_{jz} (I_{k+} + I_{k-}) \right] \right]$$

where

$$A_{jk\rho} = \widetilde{A}_{jk} + \tfrac{1}{2}(3\cos^2\theta - 1)(A_{jk} - \widetilde{A}_{jk})$$

$$B_{jk\rho} = \tfrac{1}{2}(3\cos^2\theta - 1) B_{jk}$$

$$D_{jk\rho} = \tfrac{1}{4} \sin^2\theta \, B_{jk}$$

$$E_{jk\rho} = \tfrac{1}{2} \sin\theta \cos\theta \, B_{jk} \qquad *$$

There are two points of immediate interest. The magneti-

zation of a spin system in a magnetic field defines a spin

temperature based on Curie's law. If a spin system is initially

in equilibrium with a static field at some temperature T and

if the static field can be reduced without changing the

---

* The coupling coefficients $\widetilde{A}_{jk}$ and $\widetilde{B}_{jk}$ are defined by
the spin-spin Hamiltonian in the lab frame.

$$\hbar H_{ss} = \sum_{j<k} \widetilde{A}_{jk} \overline{I}_j \cdot \overline{I}_k + \widetilde{B}_{jk} \left\{ I_j \cdot I_k - 3 \frac{(\overline{I}_j \cdot \overline{r}_{jk})(\overline{I}_k \cdot r_{jk})}{r_{jk}^2} \right\}$$

The constants A_{jk} and B_{jk} are defined in terms of
these by the relations,

$$A_{jk} = \widetilde{A}_{jk} + \tfrac{1}{2} \widetilde{B}_{jk} (3\cos^2\theta_{jk} - 1), \quad B_{jk} = -\tfrac{3}{2} \widetilde{B}_{jk} (3\cos^2\theta_{jk} - 1)$$

For a complete discussion, a reference is Abragam
pp. 546-548.

magnetization we say that the temperature is lower than before.
It happens that if there is no spin-lattice relaxation the
total static magnetization can be made to precess about the
much smaller H_{eff} in the rotating frame, a process known as
adiabatic fast passage. This means that the ratio of the
lattice to spin temperature is of the order of magnitude $\frac{H_o}{H_{eff}}$.
An exact calculation shows:

$$\frac{T_l}{T_s} = \frac{H_{eff} H_o \cos \theta}{H_{eff}^2 + 2 H_L'^2} \tag{1.8}$$

where H_L' is the local field in the rotating frame. From
Curie's Law the magnetization in the rotating frame is

$$M = \frac{M_o H_{eff} T_l}{H_o T_L} \tag{1.9}$$

The second point is that the resonant line width in the
rotating frame should be dependent on the term $(3\cos^2\theta -1)^5$
The dependency is such that the linewidth should narrow as
$(3\cos^2\theta -1)$ goes to zero or 54.7°. This effect should serve
as a test for the applicability of the spin temperature
theory in this form to individual systems.

The initial experiments of Redfield detected large
dispersion signals at rf field strengths higher than needed
to ensure the saturation of the absorption signal. The spin
system was the nuclei of Na^{23} in $NaCl^6$. He also observed
what he termed "rotary saturation" by applying an audio
frequency field perpendicular to H_{eff} in the rotating frame.
When the nuclear spin system was at resonance a decrease in
the dispersion derivative signal was observed when the audio
frequency ω_a satisfied the condition $\omega_a = \gamma H_{eff}$. In this

experiment the H_1 field was strong enough to ensure saturation. Since the results of these experiments could not be satisfactorily explained by the usual phenomemological Bloch equations Redfield introduced the concept of spin temperature. Subsequently Redfield's theory has been applied successfully to many nuclear resonance experiments, especially those involving high enough H_1 fields to cause saturation.

Enga[8] applied these ideas to electron spin resonance. As the energy of interaction of an electron spin with a magnetic field is about 1000 times greater than the interaction of a typical nuclear spin in the same field, the frequency of the analogous fields used in Enga's experiment were three orders of magnitude larger than those used by Redfield. This fact enabled Enga to use a marginal oscillator operating in the megacycle region to directly monitor changes of magnetization along H_{eff} . The spin system used was the free radical in Dpph, an organic compound with well known paramagnetic resonance properties. Dpph has a usual e.s.r. linewidth of about four gauss. Therefore his experiments were confined to fields (H_{eff}) in excess of three gauss. This corresponds to a radio frequency (rf) of approximately ten megacycles. When he applied an rf field along H_0 in addition to the microwave field perpendicular to H_0 he observed a resonance when $|H_{eff}| = \frac{\omega}{\gamma}$. This has two solutions as:

$$|H_{eff}| = [(H_0 - \frac{\omega}{\gamma})^2 + H_1^2]^{1/2} \quad \text{and this is satisfied for,}$$

$$\sqrt{H_{eff}^2 - H_1^2} = (H_0 - \frac{\omega}{\gamma})^2 \quad \text{or} \quad H_0 - \frac{\omega}{\gamma} = \pm \sqrt{(\frac{\omega_{rf}}{\gamma})^2 - H_1^2}$$

$$(1.10)$$

These two lines were observed with the expected symmetry.
The line for highest H_o was absorptive and that for lowest H_o was
emissive. This would correspond to the fact that the magnet-
ization should be parallel and antiparallel to the H_o field
direction in the two cases respectively. In addition to
these two lines an interesting center line was observed
corresponding to $H_{eff} = H_1$. As this center line had no ready
interpretation in terms of the theory proposed it was decided
to investigate this rotating frame experiment using a different
spin system. Neutron irradiated lithium fluoride crystals
seemed a good system because very narrow conduction e.s.r.
lines had been observed[9] and the crystals had a high melting
temperature. Dpph crystals would melt under the strong
absorption of power from the klystron used in this experiment
and it was proposed that the melting was in some way respon-
sible for the anomalous center line.

2. THEORY

The LiF samples used had a peak to peak derivative e.s.r. linewidth of approximately .35 gauss. It is well known that the peak to peak derivative width is related to the half power resonance curve width by $\Delta H_{pp½} = \frac{\Delta H_{½}}{\sqrt{3}}$. The characteristic spin-lattice relaxation time can be found from the half width of the absorption peak. Using the uncertainty principle $\Delta E \Delta T = \hbar$ and interpreting ΔT as the characteristic time for relaxation of a spin to the lattice gives:

$$\mu \, \Delta H_{½} \, \Delta T_{½} = \hbar \qquad (2.1)$$

where μ is the magnetic dipole moment of the electron.

Thus:
$$T_{½} = \frac{\hbar}{\mu \, \Delta H_{½}}$$

$$T_{½} = \frac{1.13 \times 10^{-7}}{\Delta H_{½}} \qquad (2.2)$$

where τ is in seconds and H is in gauss. These expressions give a relaxation time of approximately 1.9×10^{-7} seconds for the measured peak to peak width of the sample. This means that the spin lattice relaxation time is shorter than the Larmor precession time. This immediately throws serious doubt upon the validity of using the conclusions of the spin temperature theory to describe the results of this experiment.

The simplest and most standard approach for most resonance experiments has been to start with the phenomenalogical equations of Bloch. Bloch's equations are:

$$\frac{d\widetilde{M}}{d\tau} = \gamma (\widetilde{M} \times \widetilde{H}) - \left(\frac{\widetilde{M}_z - M_{0z}}{T_1}\right) - \left(\frac{M_\perp - M_{0\perp}}{T_2}\right) \qquad (2.3)$$

where M is the magnetization, H is the total instantaneous

field and $\gamma=1.76 \times 10^{7}$ oe^{-1} sec.$^{-1}$ is the gyromagnetic ratio of the electron. When one has large perturbing fields and the sample is such that $\tau = \tau_1 = \tau_2$, the Bloch equations are modified to the form,

$$\frac{d\bar{M}}{d\tau} = \gamma(\bar{M} \times \bar{H}) - (\bar{M} - \frac{x_o \bar{H}}{\tau}) \qquad (2.4)$$

The microwave field is linearly oscillating and is perpendicular to H_o. The radio frequency field is parallel to H_o and is also linearly oscillating, thus $H = H_1 \cos \omega t + \hat{k}(H_o + H_{rf} \cos \Omega t)$ This form of the Bloch equations has been used before in interpreting low field e.s.r. results.[10,11] The resonance is detected along H_{eff} in the rotating frame so we must transform this equation into the rotating frame by taking H_z as $(H_o - \frac{\omega_o}{\gamma})\hat{k}$

and $H_\perp$ as $\hat{i} H_1$. Relaxation is still assumed towards H_o because of the strong spin lattice coupling. The equation to be solved is: $\frac{dM}{d\tau} = \gamma(\bar{M} \times [\hat{k}(H_o - \frac{\omega_o}{\gamma}) + \hat{i} H_1]) - \{\bar{M} - x_o[\hat{k}(H_o + H_{rf} \cos \omega t + \hat{i}(H_1 \cos \Omega t)]\} \quad (2.5)$ This equation can not be solved exactly and since the magnetization is periodic it is effacacious to use a Fourier expansion.[12]

Setting $\bar{M} = \sum_{n=0}^{\infty} \bar{M}_n e^{in\Omega t}$ (2.6)

where obviously $\bar{M}_n = \bar{M}_{-n}^{*}$

and substituting 2.6 into 2.5 gives the iteritive eq.

$$(in\Omega - A)\bar{M}_n - B(\bar{M}_{n-1} + M_{n+1}) + \bar{C}_n = 0 \qquad (2.7)$$

where the matrices A and B are defined so that

$$A \bar{M}_n = \gamma \bar{M}_n \times \bar{H}_{eff} - \bar{M}_n / \tau \qquad (2.8)$$

$$B \bar{M}_n = \gamma \bar{M}_n \times \bar{H}_{rf} \qquad (2.9)$$

and where $H_{eff} = \hat{i} H_1 + \hat{k}(H_o - \frac{\omega_o}{\gamma})$

To use these equations they must be written out explicitly. I give enough here so that all the others are apparent. There are clearly 6n equations as there is a real and imaginary component of the magnetization; e.g.,

$$M_n^x = M_n^{xR} + i\, M_n^{xI} \qquad (2.10)$$

The equations are:

1. $M_0^{xR} - \gamma T M_0^{yR} H_\ell - 2\gamma H_m T M_1^{yR} = \chi_0 H_1 \qquad (2.11 - 2.29)$

2. $M_0^{xI} - \gamma T H_\ell M_0^{yI} = 0$

3. $M_0^{yR} + \gamma T M_0^{xR} H_\ell + 2\gamma T H_{rf} M_1^{xR} - \gamma T M_0^{zR} H_\perp = 0$

4. $M_0^{yI} + \gamma T H_\ell M_0^{xI} - \gamma T H_\perp M_0^{zI} = 0$

5. $M_0^{zR} + \gamma T H_\perp M_0^{yI} = \chi_0 H_0$

6. $M_0^{zI} + \gamma T H_\perp M_0^{yI} = 0$

7. $M_1^{xR} - \Omega T M_1^{xI} - \gamma T H_\ell M_0^{yR} - \gamma T H_{rf}(M_0^{yR} + M_2^{yR}) = 0$

8. $M_1^{xI} - \Omega T M_1^{xR} - \gamma T H_\ell M_0^{yI} + \gamma T H_{rf}(M_0^{yI} + M_2^{yI}) = 0$

9. $M_1^{yR} - \Omega T M_1^{yI} - \gamma T M_1^{zR} H_\perp + \gamma T H_\ell M_1^{xR} + \gamma T H_{rf}(M_0^{xR} + M_2^{xR}) = 0$

10. $M_1^{yI} + \Omega T M_1^{yR} - \gamma T H_\perp M_1^{zI} + \gamma T H_\ell M_1^{zI} + \gamma T H_{rf}(M_0^{xR} + M_2^{xR}) = 0$

11. $M_1^{zR} - \Omega T M_1^{zI} + \gamma T H_\perp M_1^{yR} = \chi_0 H_{rf}$

12. $M_1^{zI} + \Omega T M_1^{zR} + \gamma T H_\perp M_1^{yI} = 0$

13. $M_n^{xR} - n T \Omega M_n^{xI} - \gamma T H_\ell M_n^{yR} - \gamma T H_{rf}(M_{n-1}^{yR} + M_{n+2}^{yR}) = 0$

14. $M_n^{xI} + n \gamma \Omega M_n^{xR} - \gamma T H_\ell M_n^{yR} - \gamma T H_{rf}(M_{n-1}^{yI} + M_{n+1}^{yI}) = 0$

15. $M_n^{yR} - n T \Omega M_n^{yI} - \gamma T H_\perp M_n^{zR} + \gamma T H_\ell M_n^{xR} + \gamma T H_{rf}(M_{n-1}^{xR} + M_{n+1}^{xR}) = 0$

16. $M_n^{yI} - n T \Omega M_n^{yR} + \gamma T M_n^{zI} H_\perp - \gamma T H_\ell M_n^{xI} - \gamma T H_{rf}(M_{n-1}^{xI} + M_{n+1}^{xI}) = 0$

17. $M_n^{zR} - n \Omega T M_n^{zI} + \gamma H_\perp M_n^{yR} = 0$

18. $M_n^{zI} + n \Omega T M_n^{zR} + \gamma T H_\perp M_n^{yI} = 0$

In the above equations $H_\ell = \left(H_0 - \frac{\omega}{\gamma}\right)$.

This suggests solving the 6n x 6n matrix equation AM=C where A is the matrix defined by the coefficients of the magnetization and M is a 6n dimensional vector representing the components of magnetization, C is another column vector representing the inhomogeneous terms in the equations. There are only three non zero terms C_1, C_5, and C_{11}. C_1 and C_{11} are three orders of magnitude smaller than C_5 and it proved to make no noticeable difference in the results to neglect these terms and retain only C_5. This is reasonable since $H_o >> H_1$ or H_{rf}. The matrix equation was solved numerically on an IBM 7040 computer. Terminating the series at n=5 and chosing fixed values for all the parameters except one which assumed five values, one machine run took 10 minutes. This was found to be sufficient for our needs as we needed only to determine M_1^{tr} or more precisely the derivative of M_1^{tr} with respect to H_o. Including the n=6 terms served to change the calculated derivative at n=5 by only one part in 10^4, regardless of the fact that the M_6 components were not negligible compared to the M_5 components.

One interesting point of the experiment is the effect on the linewidth when increasing the angle between H_{eff} and H_o. It was noted in the introduction that the linewidth in the rotating frame should narrow as the function $3\cos^2\theta - 1$ becomes smaller if the spin temperature hypothesis is valid for the case. The prediction of our theory is not immediately apparent but when a constant τ is used in the equations the

linewidth should be constant in the rotating frame. The
relation of the linewidth along H_{eff} to that in the lab frame
is simple as long as the linewidth is small compared to H_{eff}.
The relation follows from equation 1.10.

$$H_{eff} = \sqrt{(H_1 - \frac{\omega}{\gamma})^2 + H_1^2}$$

$$\Delta H_{eff} = \frac{(H - \frac{\omega}{\gamma})\, \Delta(H - \frac{\omega}{\gamma})}{\sqrt{(H - \frac{\omega}{\gamma})^2 + H_1^2}} \qquad so \qquad \Delta H_{eff} = \Delta(H - \frac{\omega}{\gamma})\cos\theta \qquad (2.30)$$

So assuming the linewidth is a constant the dependence of the
measured linewidth in the lab frame should be $\frac{\Delta H_{1/2}}{\cos\theta}$. It is
unfortunate that the highest values of H_1 obtainable were only
around one gauss which is not large enough to test this pre-
diction accurately. For large angles, $H_{eff} \approx$ one gauss which is
not much larger than the linewidth. Since the computer results
matched the experimental lines for all cases observed it was
run for a series of angles with $H_{eff} \approx 10\ H_{1/2}$. This plot is
given along with a plot of $\frac{\Delta H_{1/2}}{\cos\theta}$ and $\Delta H_{1/2}(3\cos^2\theta - 1)$ in figure 19.

3. APPARATUS

The apparatus consists of a high power 34 GHz Elliot type 8TFK2 klystron capable of 10 watts output, an isolator, load, and associated microwave equipment including a TE104 retangular cavity, a bolometer and Hewlett Packard Model 430C power meter, a field controlled 9.5 inch Magnion magnet along with field modulation equipment, two marginal oscillators, a Hewlett Packard frequency counter, a lock-in detector. Chart recorder and the auxiliary equipment needed for stabilization. The arrangement is shown in the block diagram (Figure 2). The klystron is water cooled providing enough stability so that it could be run satisfactorily without an a.f.c. after an initial warm up period of half an hour. The klystron could not be swept through an entire mode and displayed on the oscilliscope as this involved modulating the beam voltage supply by about 150 volts. In practice then the a.f.c. was not used and the klystron was allowed to drift slightly. This meant retuning the klystron to the cavity frequently. This was accomplished in two steps. First a rough setting of the frequency was obtained through the calibrated wavemeter. Then the klystron was fine tuned until the maximum signal strength was obtained. The frequency could be found to about ten MHz with the wavemeter. The coupler is described in detail in
Enga's thesis. While the strength of the field can be controlled through the coupling there is no calibration and the settings

are not reproducible. The cavity used was the same as
described in Enga's thesis and although the silver plating had
deteriorated the Q was not seriously affected. The cavity
was also cooled through an external copper tube affixed to
the side of the cavity. Details of the cavity and teflon
sample holders are shown in figure 4. The sample coil size
depended on the frequency desired but coils made of 100
turns of no. 46 enameled copper wire oscillated at about three
MHz. The other microwave equipment is described in detail
in Enga's thesis. A schematic of the klystron power supply
and its connections to the klystron is shown in figure 7.
The power supply is noisy and detection of e.s.r. by
monitoring power absorbed from the microwave system would
be difficult. An additional difficulty was that the klystron
mode could not be displayed thus making it difficult to match
the klystron frequency to the cavity resonant frequency.
A Hewlett Packard frequency counter with a 50-100 MHz plug
in unit was used to determine the exact frequencies for the
e.s.r. resonance along H_{ess} and the proton resonance
frequency in H_0. Using the plug in unit frequencies both
above and below 50 MHz can be determined by changing the
selector knob. This avoids the necessity of two counters.

The marginal oscillator is a slightly modified form
of the one described by Benedek and Kushida[14] and Volkoff
et al.[15] The 6J6 tube operates as a push-pull oscillator with
the resonant frequency determined by the sample coil and

butterfly tuning capacitors. The grid-plate feedback capac-
itors are adjusted for marginal oscillation. At resonance,
energy is absorbed from the sample coil changing its Q and
hence changing the current delivered to the circuit via the
plate supply. This signal is modulated by the Helmholtz
modulation coils at ω and is fed via a coaxial cable to the
lock-in detector. This in turn is connected to a chart
recorder. A transistorized audio amplifier connected to the
plate circuit is used to monitor the frequency. It provides
enough gain to drive the Hewlett Packard model HP5245 L frequency
counter. This amounts to over .1 volt at the frequencies used.
The d.c. meter on the front of the marginal oscillator
essentially measures the voltage developed by the grid
current across a 51 K resistor on the positive half of the
wave form. See figure 3. The small grid capacitors can be
used to adjust the grid voltage and hence the d.c. field
strength. The unmodified oscillator was capable of operating
between about 5 and 60 MHz. For operation at lower frequencies
extra capacitance was added to the grid capacitors. With a
coil of about 100 turns and a capacitor in parallel with the
grid trimmer of 47 pf a frequency of 3 to 3.5 MHz could be
obtained. A parallel capacitance of 100 pf would give freq-
uencies down to 2.3 MHz. However at such frequencies the
tuning range of the oscillator was limited to a few hundred
kilocycles. To obtain all desired frequencies from 2.3 to 4
MHz it was necessary to use two spectrometers, one modified

and one unmodified, and two spectrometer to signal coil cable
lengths. When operating properly the signal to noise ratio
of the oscillator was over 100 for the n=1 resonance line in
LiF. The physical construction of the oscillator is discussed
in Enga's thesis, and a schematic diagram is given in figure 3.
Figure 6 contain diagrams of the cavity coupling mechanism
and a TE011 mode cylindrical cavity. This cavity was not
used in the present experiments but was used by Enga in his
original experiments and so is included for completeness.
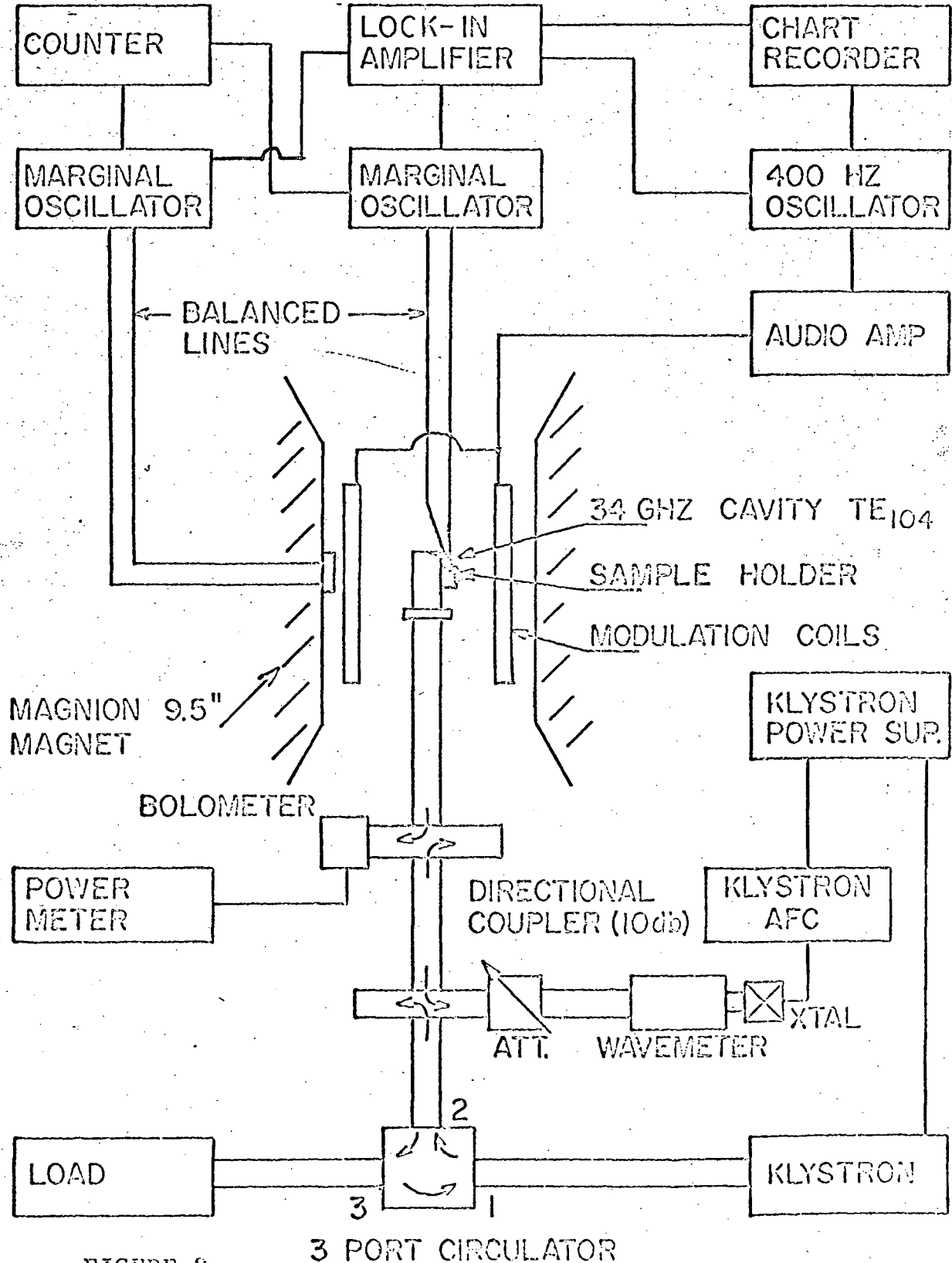
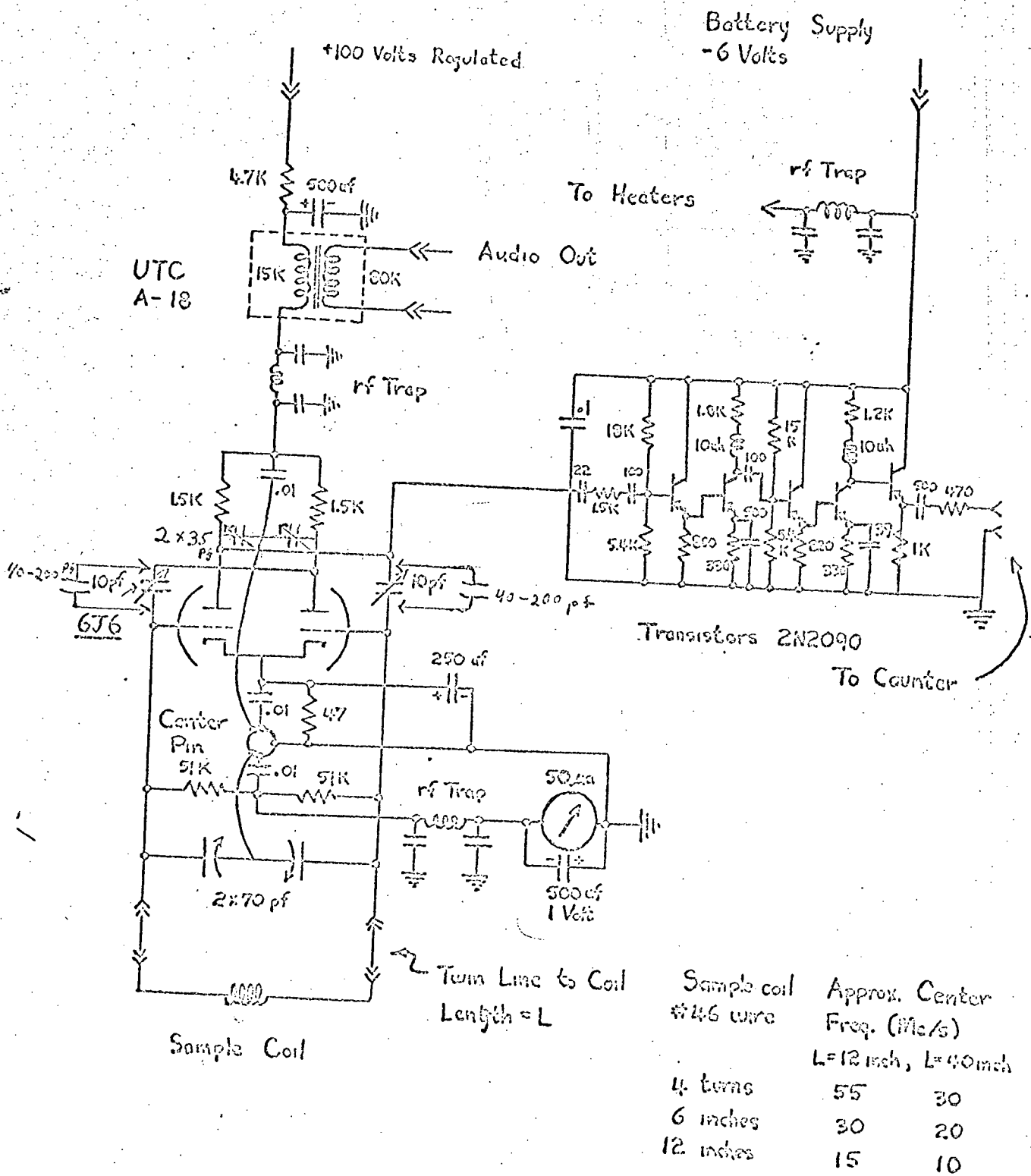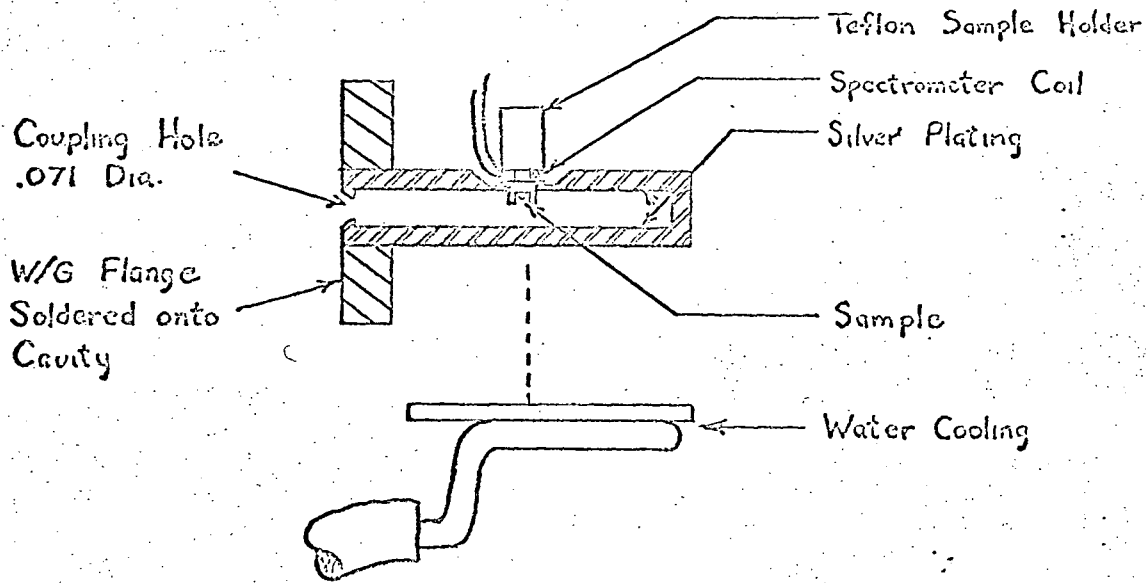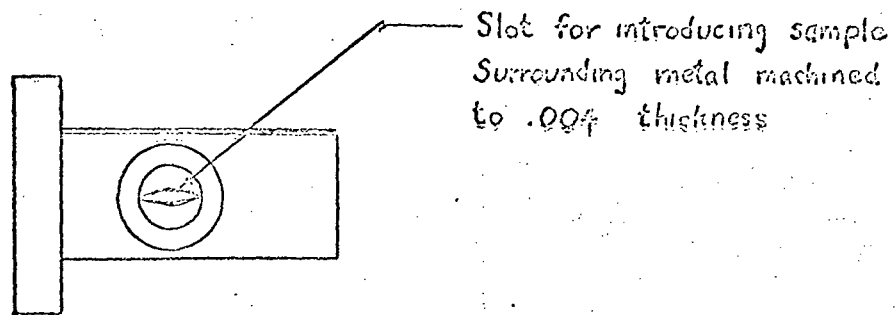BLOCK DIAGRAM OF THE EXPERIMENTAL APPARATUS

FIGURE 2

3 PORT CIRCULATOR

FIG. 3. Spectrometer Circuit

Teflon Sample Holder

Spectrometer Coil

Silver Plating

Coupling Hole
.071 Dia.

W/G Flange
Soldered onto
Cavity

Sample

Water Cooling

SIDE VIEW CUTAWAY

Slot for introducing sample
Surrounding metal machined
to .004 thickness

TOP VIEW

.071 Dia.

.140

.832

.200

R=.218

.050

.441

.100 Dia.

.025

.010

.030

.050 Dia.   .055

#60 Drill
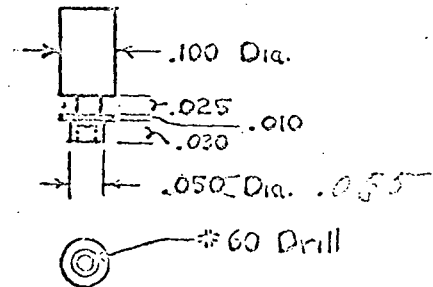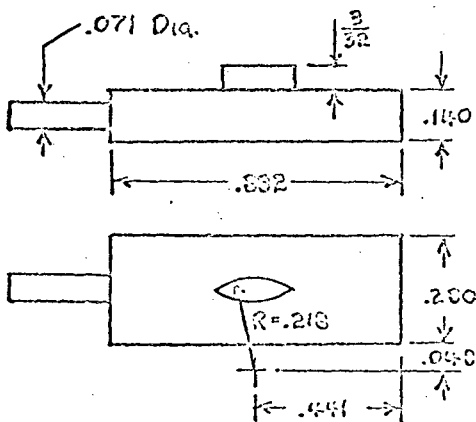
LUCITE PLASTIC FORM ON WHICH
CAVITY WAS ELECTROPLATED

SAMPLE BOBBIN (TEFLON)

FIG. 4.   TE 014 MODE CAVITY (RECTANGULAR)

FIG. 5. Klystron Freq. Stabilizer
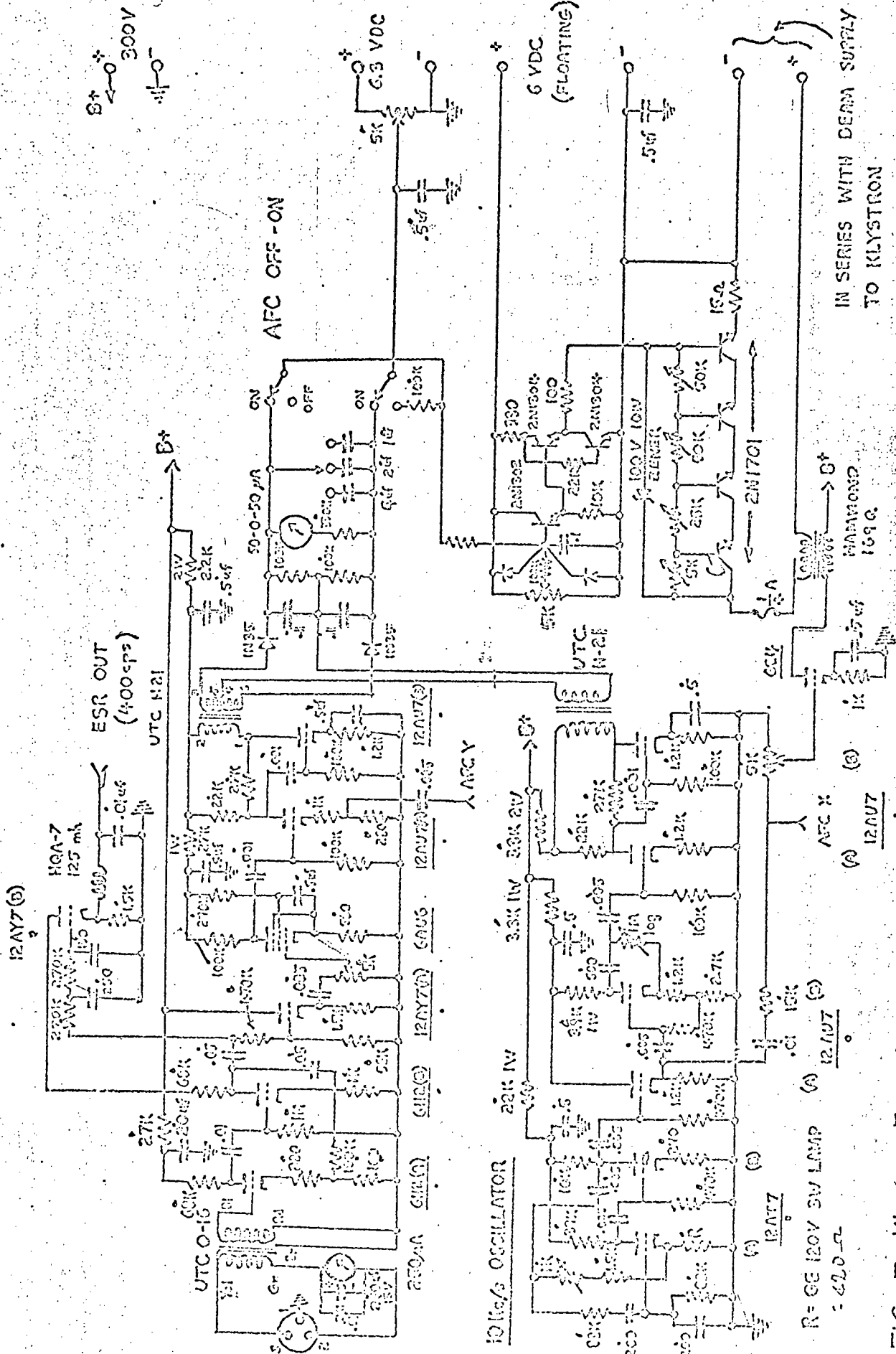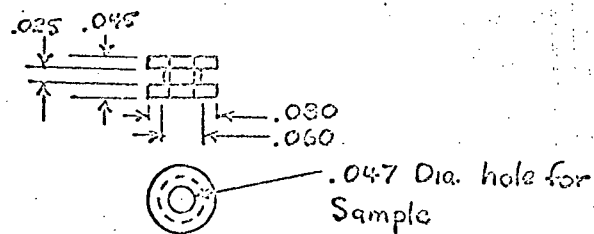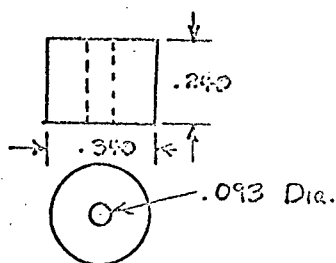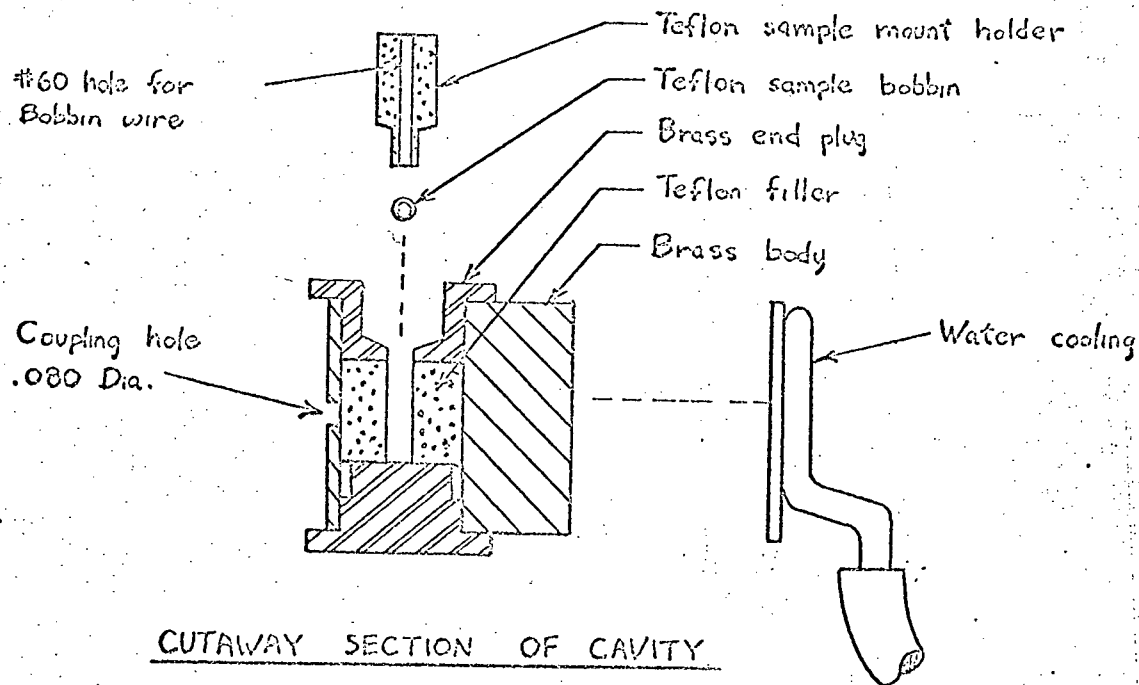
#60 hole for Bobbin wire

Teflon sample mount holder
Teflon sample bobbin
Brass end plug
Teflon filler
Brass body

Coupling hole .080 Dia.

Water cooling

CUTAWAY SECTION OF CAVITY

.240

.340

.093 Dia.

TEFLON FILLER

.025 .045

.080
.060

.047 Dia. hole for Sample

SAMPLE BOBBIN (TEFLON)

FIG. 15   TE 011 MODE CAVITY

Flange   Brass Inserts   Flange   Teflon slider insert

.17

WR-22 W/G

Slot for moving Teflon insert

.5   .7   .8   .7

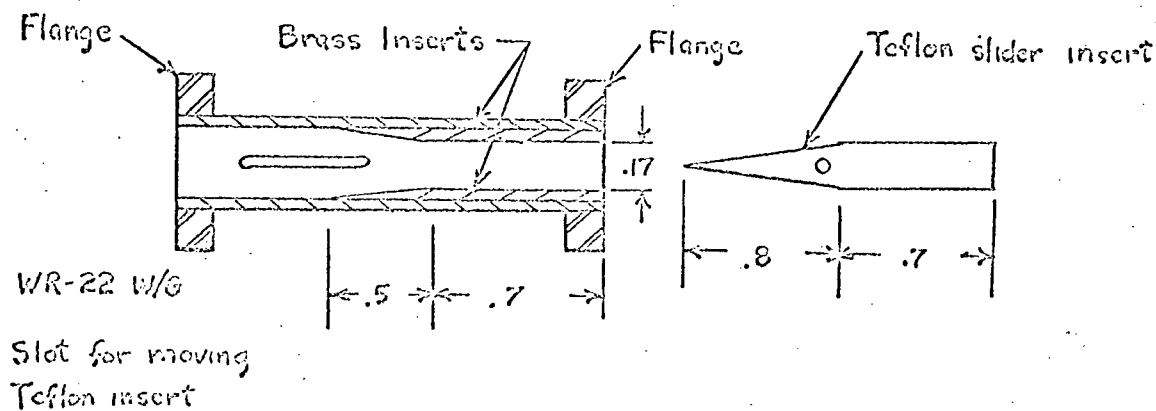CUTAWAY VIEW SHOWING BRASS INSERTS IN WR-22 W/G

FIG. 6. VARIABLE COUPLING DEVICE

BLOCK DIAGRAM OF KLYSTRON SUPPLY

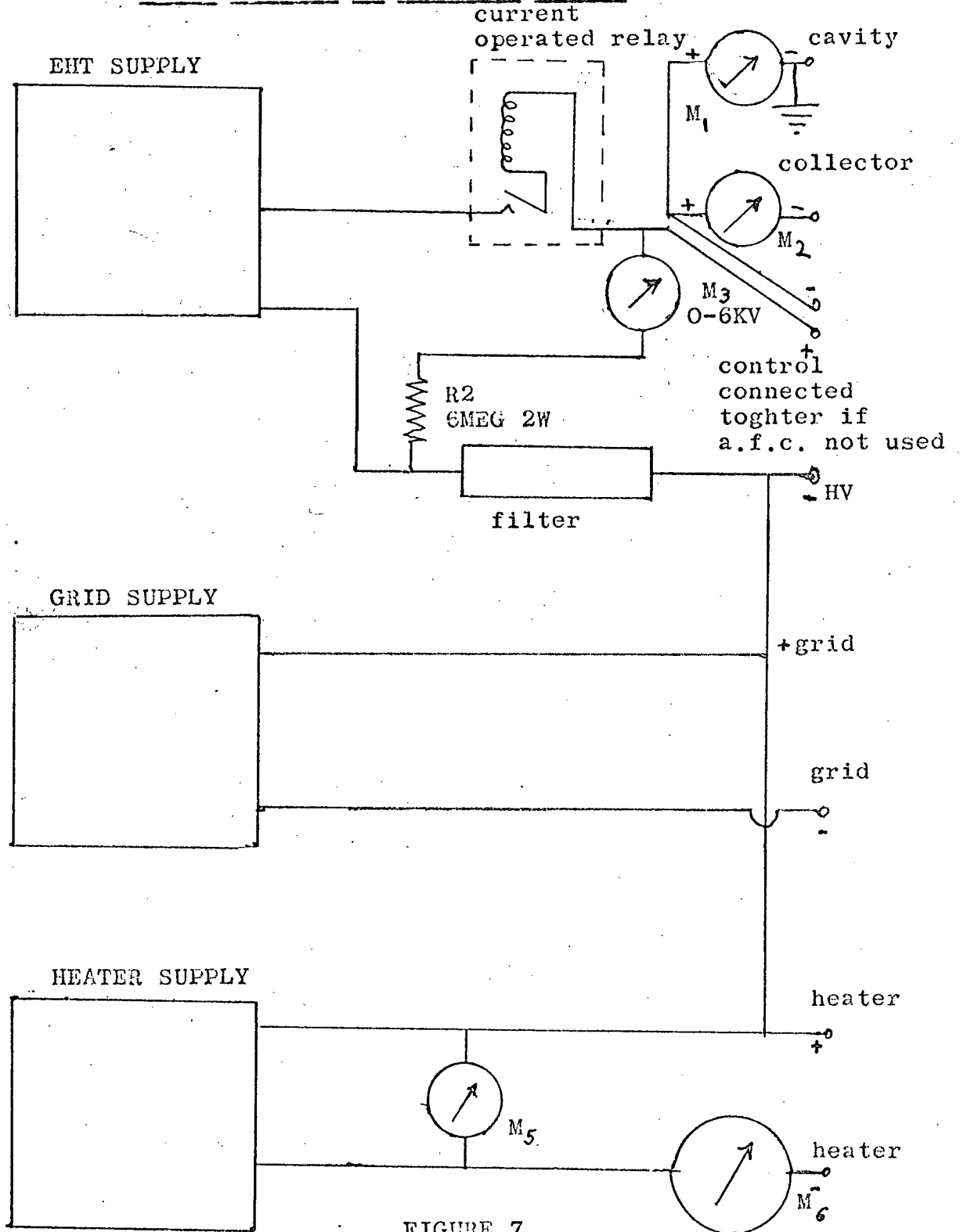FIGURE 7

4. EXPERIMENTAL PROCEDURE AND RESULTS

The experiments were carried out at room temperature in all cases. The static magnetic field H_o was modulated at 400 Hz. and a lock-in detection system was employed. The signals were obtained by setting the klystron at a fixed frequency corresponding to the cavity resonance and setting the marginal oscillator for the frequency which gave the desired H_{eff} and then slowly sweeping H_o via the calibrated sweep power supply. Typical sweep speeds were of the order of a few gauss per minute. The derivative signals were displayed on a chart recorder. Preliminary runs were first made at frequencies greater than 6 MHz. For these runs lines similar to those found by Enga were observed. Figure 8 shows typical traces taken at these frequencies.
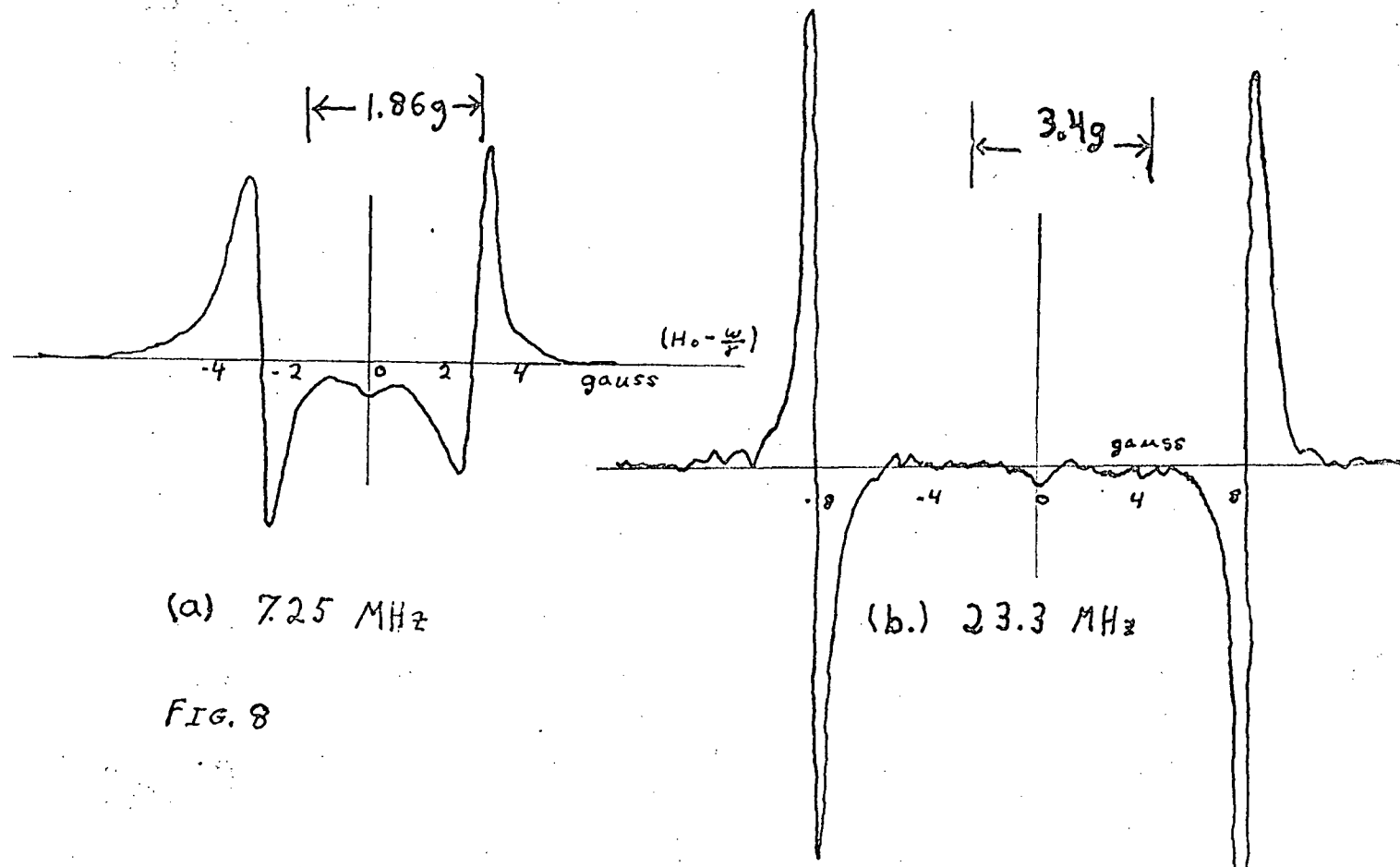

(a) 7.25 MHz

(b.) 23.3 MHz

FIG. 8

Fig. 9 shows the qualitative effect of increasing H_1 through
increasing the coupling to the cavity. All these runs were at
3.58 MHz and approximately 10 to 14μA of oscillator meter reading
which indicates the rf field strength. H_1 increases from (a)
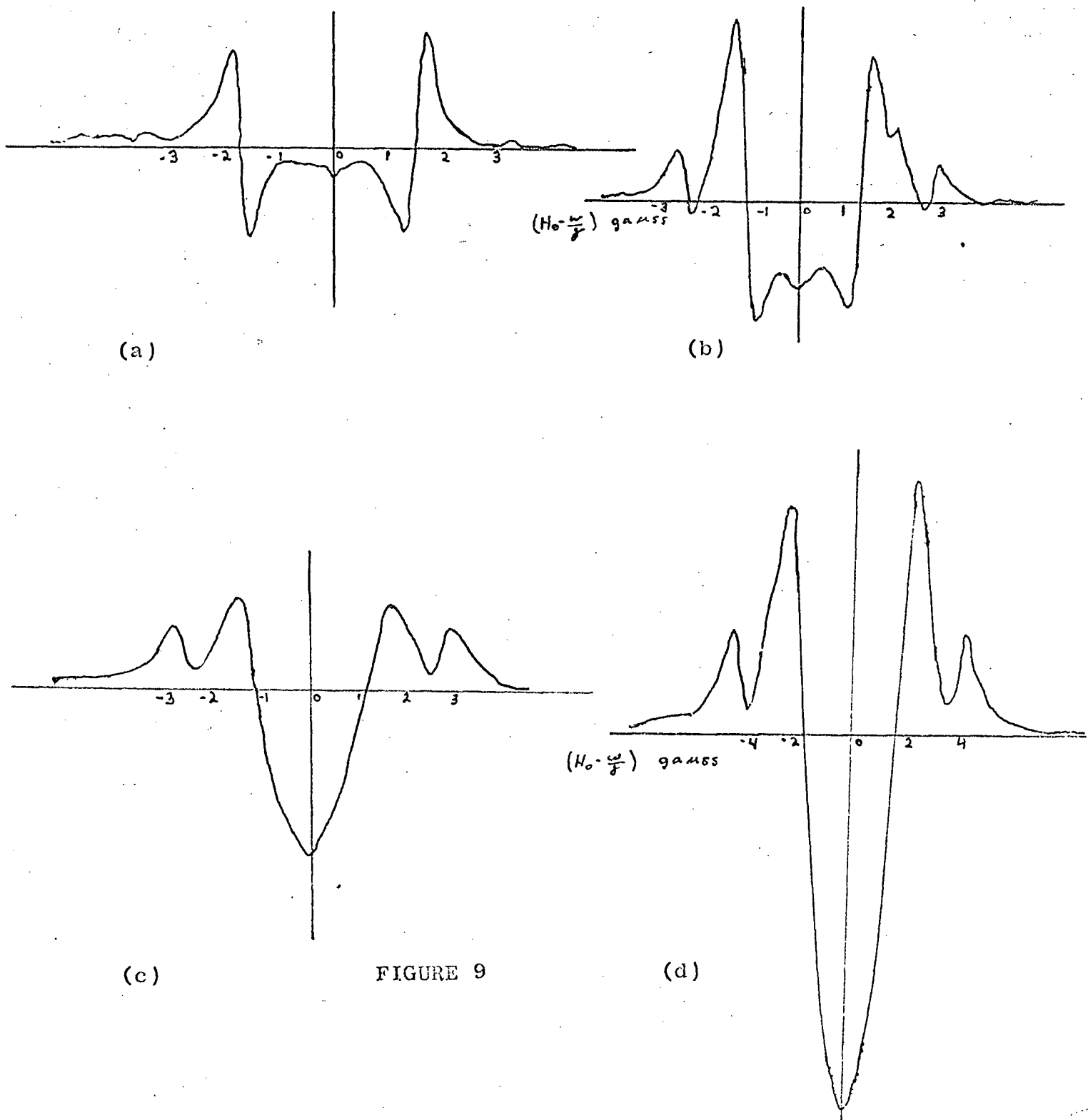through (d) but no accurate quantitative values for H_1 were
obtained for these runs.

(a)

(b)

$(H_o - \frac{\omega}{g})$ gauss

(c)

FIGURE 9

(d)

$(H_o - \frac{\omega}{g})$ gauss

In fig.10 all the signals were obtained at a frequency of 2.6 MHz. The current reading reflects the relative strength of H_{rs} but H_1 is not calibrated. Figure (b), however, has the largest value of H_1.

(a)   5-7 µA
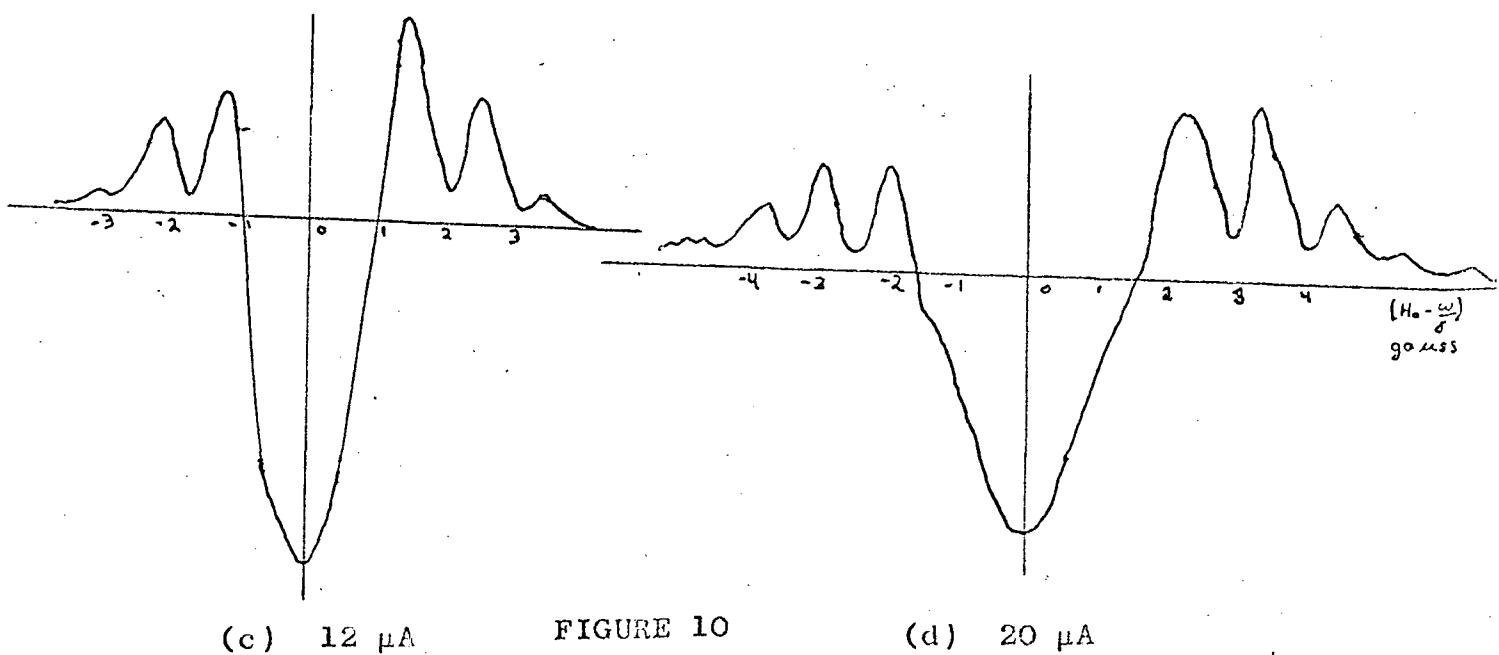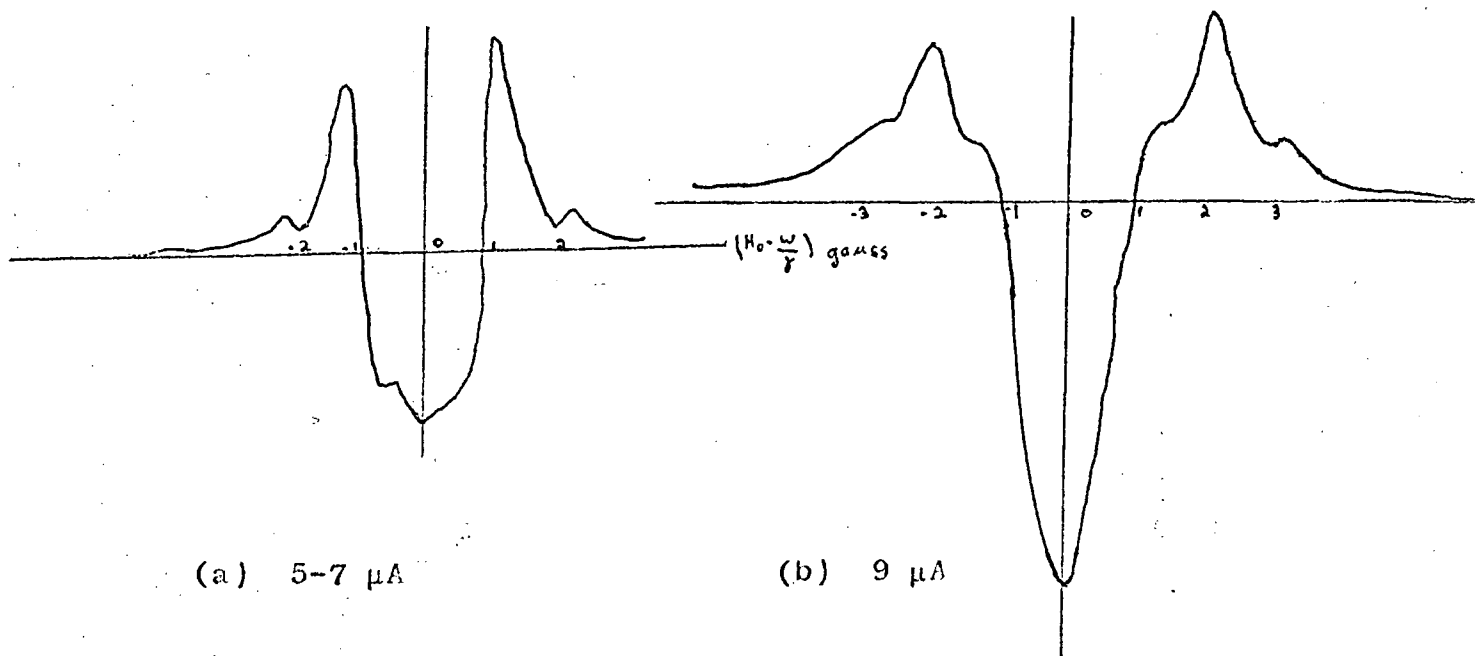
(b)   9 µA

(c)   12 µA   FIGURE 10   (d)   20 µA

The magnetic field was not calibrated in these prelim-
inary runs but from the calibration obtained in subsequent
runs it was apparent that at these oscillator frequencies
the microwave field strength was small compared to H_{eff}.
In the usual first treatment of resonance the equation for
the evolution of the magnetization,

$$\frac{d\overline{M}}{dt} = \gamma \overline{H} \times \overline{M} \qquad (4.1)$$

is solved exactly by separating H into the vector components:

$$\overline{H} = \hat{k} H_0 + \hat{i} H_1 \cos \omega t + \hat{j} H_1 \sin \omega t$$

This implies that the perpendicular rf field is rotating about
H_0. Obviously a linearly oscillating field $2H_1 \cos \omega t$ can
be decomposed into two oppositely rotating magnetic fields.

$$H_R = \hat{i} H_1 \cos \omega t + \hat{j} H_1 \sin \omega t$$

$$H_L = \hat{i} H_1 \cos \omega t - \hat{j} H_1 \sin \omega t$$

If H_0 is large compared to H_1 it can be shown that only one
rotating component is important toward effecting a resonance.
Hence when H_1 is small compared to H_0 a linearly oscillating
rf field may be treated as a rotating field. Doing this, only
one condition for resonance is possible and this occurs
when $H_0 = \frac{\omega_{rf}}{\gamma}$ and $2\pi\omega_{rf}$ corresponds to the Larmor precession
frequency. In actual practice a linearly oscillating field
is almost always used. In this experiment the linearly
oscillating rf field was comparable in strength to H_{eff} for
low frequencies of Hrf and high rf field strengths. In this
case it is no longer proper to neglect one of the rotating
components of the field. In fact an analysis of the fields

present in the doubly rotating frame (the one rotating about
the axis defined by H_{eff}), shows that there are other resonance
conditions than the one given above. Winter's analysis[16]
shows that for a rf magnetic field with non zero components
in all of the coordinate directions resonant conditions exist for
$\omega = n\omega_0$ where ω_0 is the Larmor precession frequency in the rotating
frame about H_{eff}. The chances of observing these higher
order resonances is greatly enhanced as the rf field strength
becomes comparable to the static field. Thus the rotating
frame possibly affords the only means to study these higher order
resonances for electron spin resonance. There are two ways
to achieve an H_{rf} large relative to H_{eff}, either require that
the oscillator produce a large oscillating field or make H_{eff}
small by using a lower rf frequency. The latter is better
because the sensitivity of the oscillator is greatest for low
field strengths. For these reasons it was decided to make runs
at as low as practical rf frequencies. A perturbation
calculation[17] shows that if the effect is small the $n=2$
resonance signal strength should be proportional to H_{rf}^{4} while
the $n=3$ resonance should be proportional to H_{rf}^{6}. Of course the
$n=1$ resonance strength is proportional to H_{rf}^{2}.

Figure 11 shows the effect of increasing H_{rf} while the other
parameters are held constant, the frequency being 2.6 MHz.
Figure 12 shows the same experiment but with $\frac{\omega_{rf}}{2\pi} = 3.0$ MHz. It
is obvious from these results that the strength of the higher
order resonances is highly sensitive to the strength of H_{rf}.

Also for the same rf field strength the strength of the higher order resonances increases as ω_{rf} decreases. This is the same as decreasing H_{eff}. A semi-quantitative description of the effect of H_{rf} strength on the relative signal strengths was made by noting that for a Lorentzian line shape the integrated area under the absorption curve is proportional to the peak height and the derivative peak height assuming that the line width is constant. This is a good approximation for the ranges of the magnetic fields used in this experiment. Figure 13 shows the results of this measurement for a typical run at 3.0 MHz. Six traces were made for H_{rf} field strengths of from 7 to 30 μA as read on the oscillator meter.[18] For each value of H_{rf} the ratio of peak height 2-to-1, 3-to-1, and 4-to-1 was measured. Only at the two highest values of H_{rf} could measurements be made for the ratio of peak 4 to peak 1. The peak heights could not be compared between one value of H_{rf} and another because the sensitivity of the oscillator is some unknown function of the oscillator signal strength. From the slope of the log log plot it is seen that:

$$\frac{I_2}{I_1} \propto H_{rf}^{2(.9 \pm .1)}$$

$$\frac{I_3}{I_1} \propto H_{rf}^{2(1.8 \pm .2)}$$

$$\frac{I_4}{I_1} \propto H_{rf}^{2(3.3 \pm .5)}$$

Within the limits of error then,

$$I_1 \propto H_{rf}^2 \quad, \quad I_2 \propto H_{rf}^4 \quad, \quad I_3 \propto H_{rf}^6 \quad \text{and} \quad I_4 \propto H_{rf}^8$$

This is what the perturbation theory for low H_{rf} would predict, although perturbation theory is definitely not applicable as $H_{rf} \approx H_{eff}$.
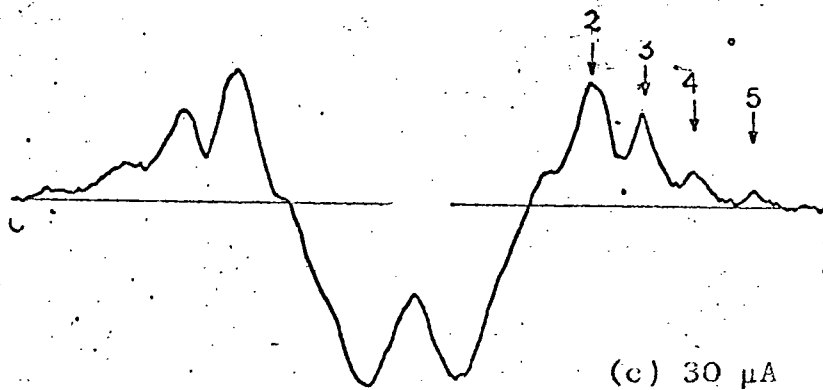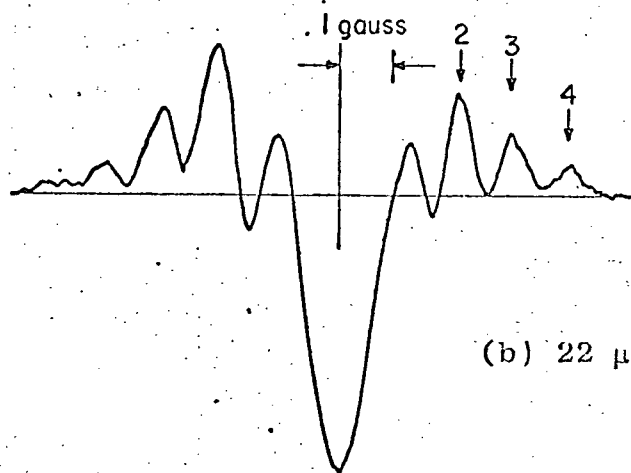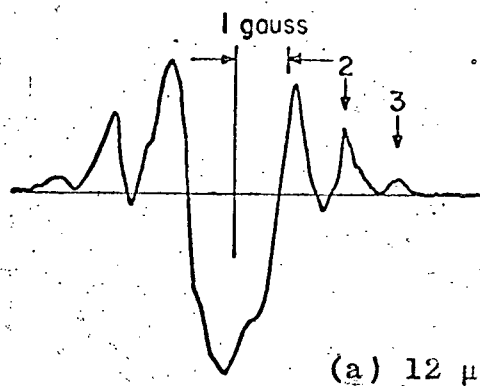
(a) 12 μA

(b) 22 μA

(c) 30 μA

FIGURE 11

SAME EXPERIMENT AS
FIG. 11 EXCEPT AT
3.0 MHz

(a) 14 μA

$\left(H_0 - \frac{\omega}{\gamma}\right)$ gauss

(b) 20 μA

$\left(H_0 - \frac{\omega}{\gamma}\right)$

(c) 30

$\left(H_0 - \frac{\omega}{\gamma}\right)$ gauss
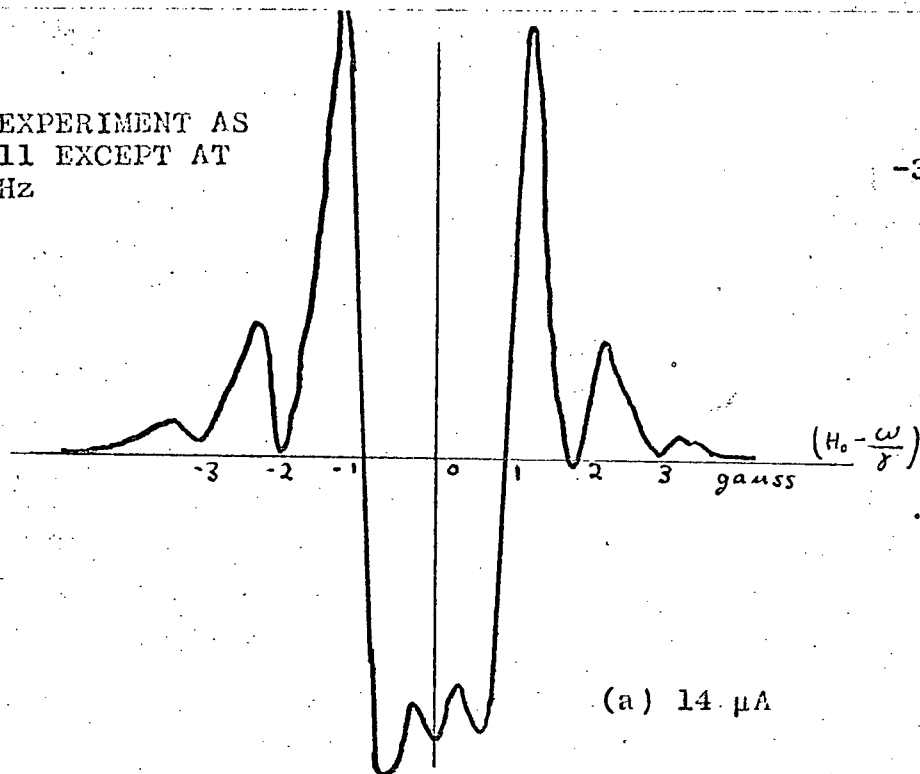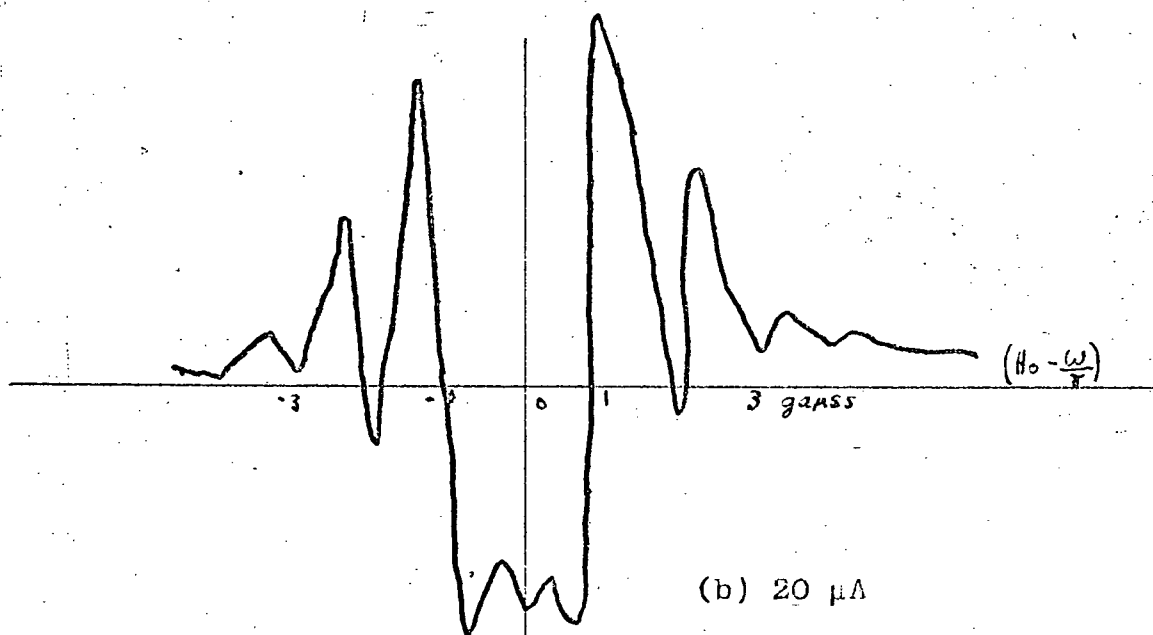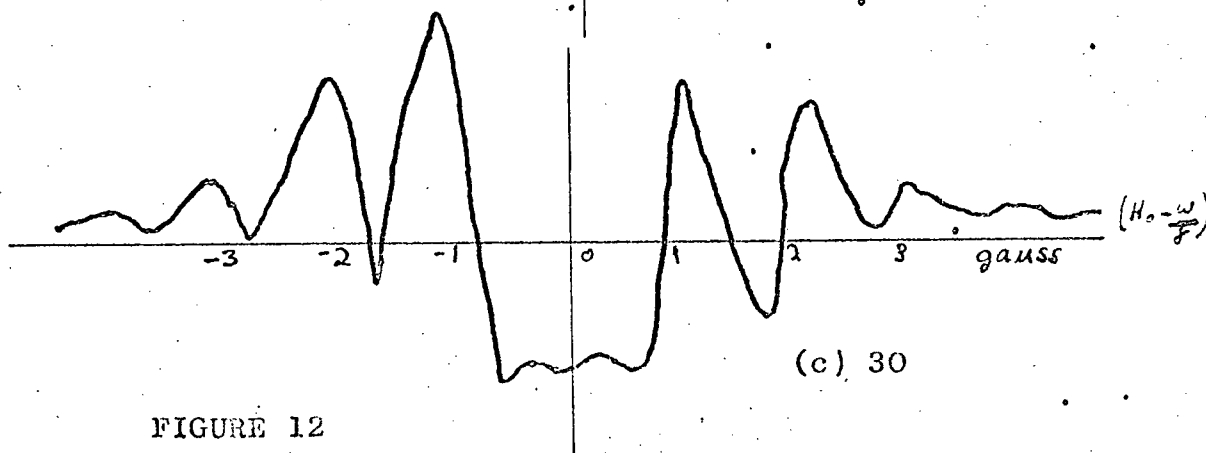
FIGURE 12

PLOT OF ln H_{rf}^2 vs ln OF RELATIVE PEAK STRENGTH
FIGURE 13

The next three figures (14-16.) show numerical solutions for the equations developed in the theory. They are plots of $\frac{d}{dH_o} M_i^{2I}$. Figure 14 shows the effect of changing the relaxation t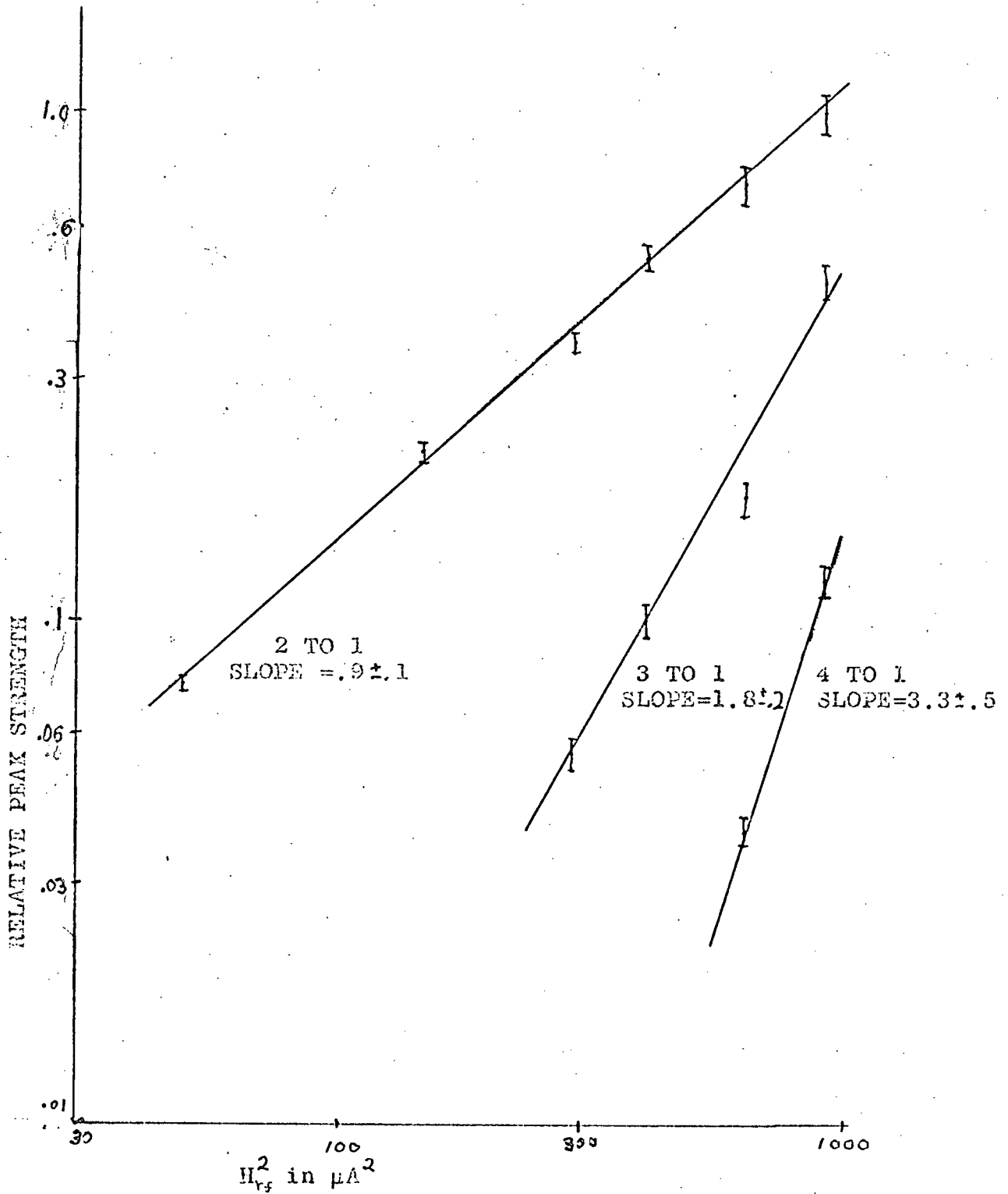ime τ. Shortening τ has the effect of broadening the resonance lines. However as will be shown other parameters can have similar effects and the broadening due to τ and that due to other effects must be distinguished if the proper τ is to be found in this manner. It will be seen that the broadening due to the fact that we are observing a rotating frame resonance in the lab is important only when $\cos\theta$ is significantly different from unity. Therefore the search for the correct value of τ should be limited to frequencies higher than 3.5 MHz and low field strengths. The result is that the best τ was found to be 1.5×10^{-7} seconds. This is comparable to 1.9×10^{-7} calculated from the peak to peak derivative line width. The discrepency could be due to the fact that the 1.9×10^{-7} second figure was derived from the unsaturated resonance line obtained from a low power klystron. All the signals were obtained in the rotating frame with H_{rf} as the perturbing field. The rather high field strengths of H_{rf} should induce significant saturation. The klystron power will not itself produce significant saturation since all of the signals were obtained at least 2 MHz or about 3 halfwidths from the klystron resonant frequency. The half width at resonance is given by:[19]

$$\Delta_{\frac{1}{2}}' = \Delta_{\frac{1}{2}} \left(1 + \gamma^2 H_{rf}^2 T^2 \right)^{\frac{1}{2}} \qquad (4.2)$$

where $\Delta_{\frac{1}{2}}$ is the unsaturated linewidth. For the γ of the electron and a τ of 1.5×10^{-7} sec. and H_{rf} of .5 gauss, $\Delta_{\frac{1}{2}}' = 1.74 \Delta_{\frac{1}{2}}$.

The observed difference, $\dfrac{1.9}{1.5}$ gives only $\Delta\frac{\nu}{2}=1.25\Delta\nu_{\frac{1}{2}}$, but the argument explains the effect qualitatively.

Figure 15 shows the effect of increasing H_1 while the other parameters are held constant, and finally, figure 16 shows the effect of increasing H_{rf}. In some respect the effects of increasing H_1 or H_{rf} are quite similar and the differences rather subtle. It is quite easy to see why the effects should be similar. Only the component of H_{rf} perpendicular to H_{eff} is effective in causing resonant absorption. This component is $H_{rf}\sin\theta$. From figure 1, $\sin\theta = H_1/H_{eff}$, so the perturbing field is actually $H_{rf} H_1/H_{eff}$ where H_{eff} is determined by ω_{rf} which is kept constant. Thus if the only component of H_{rf} were along the z axis the effects on the peak height due to H_1 and H_{rf} would be indistinguishable. Experimentally however there is always a component of H_{rf} in the x-y plane and this component probably accounts for the differences in the lineshape observed even when the product $H_{rf} H_1$ is kept constant. Of course H_1 effects the angle θ and thus the separation of the absorptive and emissive resonance lines. H_{rf} has no such effect.

Figures 17 and 18 show a comparison of the theoretical and experimental curves for some typical runs. The parameters in the theoretical curves have been chosen to give the best fit to the experiment. Figure 17 shows runs at two frequencies while the other parameters are held constant. The main effect is clearly a change in relative peak heights. The parameters

THE THEORETICAL EFFECT OF CHANGING τ

$\Upsilon = 2.6 \times 10^{-7} \text{ SEC}$
$\mathcal{F} = 3.5 \text{ Mc}$
$H_1 = .50 \text{ g}$
$H_{rs} = .45 \text{ g}$

$\Upsilon = 1.8 \times 10^{-7} \text{ SEC}$
$\mathcal{F} = 3.0 \text{ Mc}$
$H_1 = .5 \text{ g}$
$H_{rf} = .6 \text{ g}$

Gauss
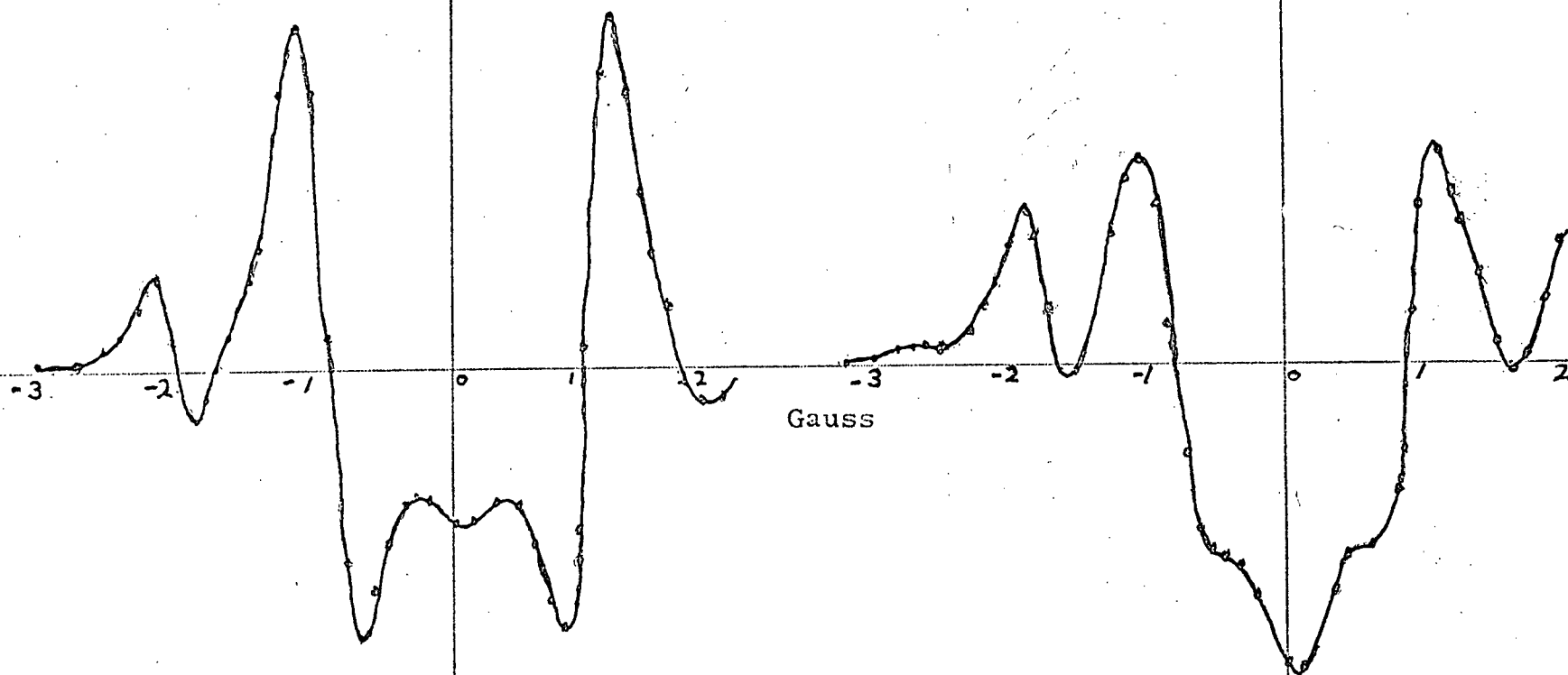
FIGURE 14

THE THEORETICAL EFFECT OF INCREASING H₁ WHILE

THE OTHER PARAMETERS ARE HELD CONSTANT

(a) $H_1 = .2g$
$H_{15} = .65g$

(b) $H_1 = .45g$
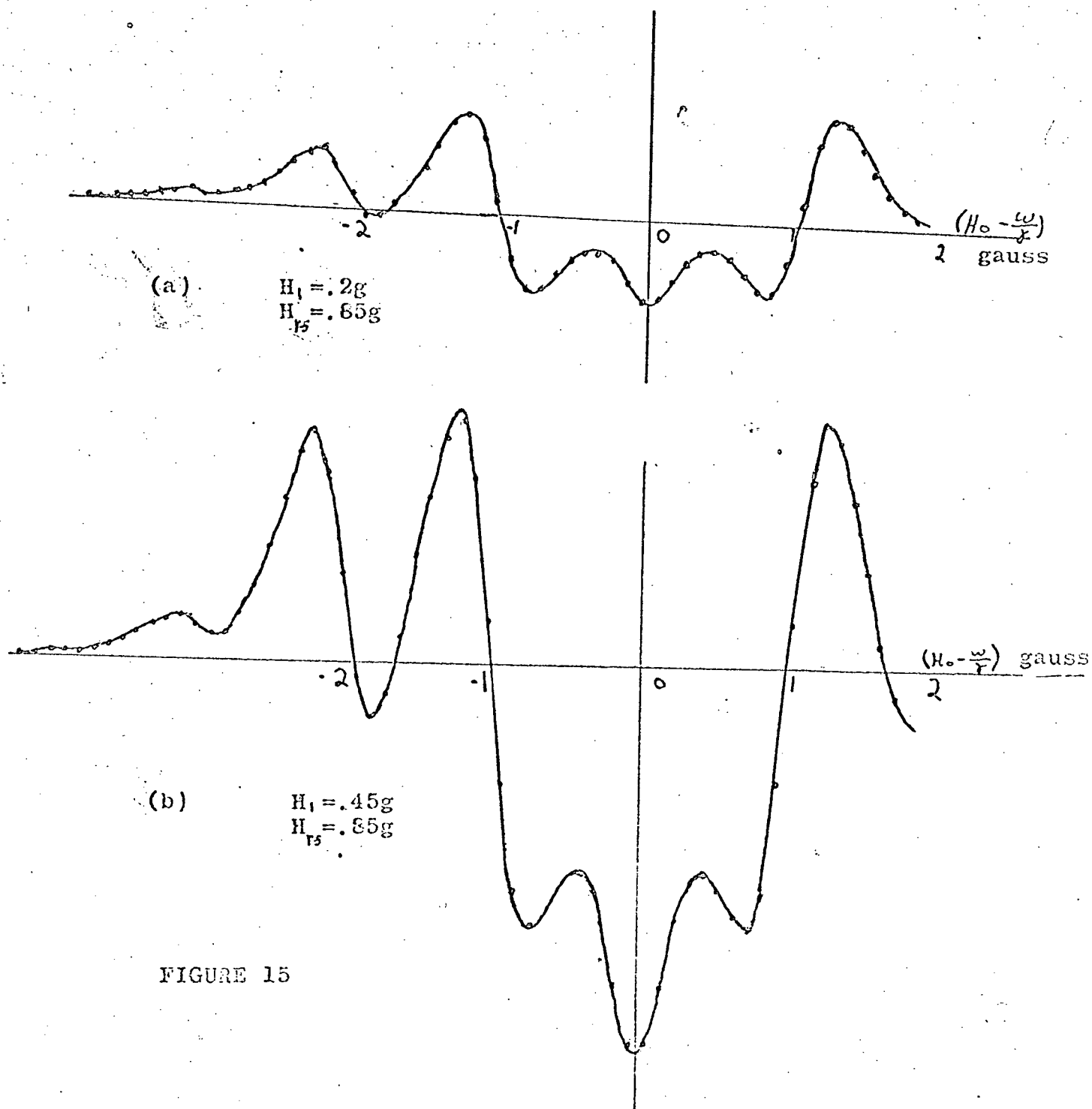$H_{T5} = .85g$

FIGURE 15

(c)

$H_1 = .7g$
$H_{rf} = .85g$

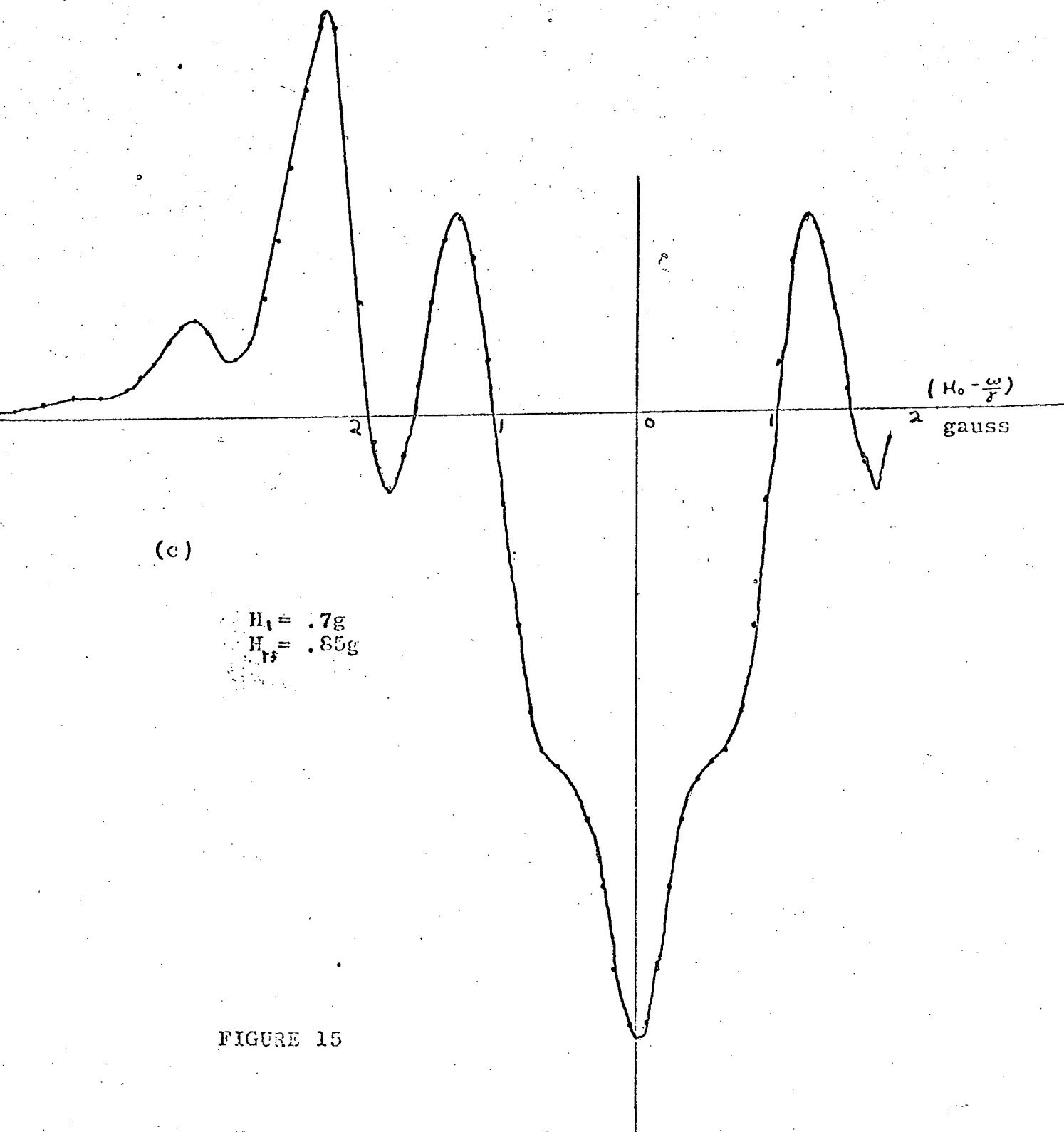FIGURE 15

THE THEORETICAL EFFECT OF INCREASING H$_{rs}$WHILE THE OTHER PARAMETERS ARE HELD CONSTANT
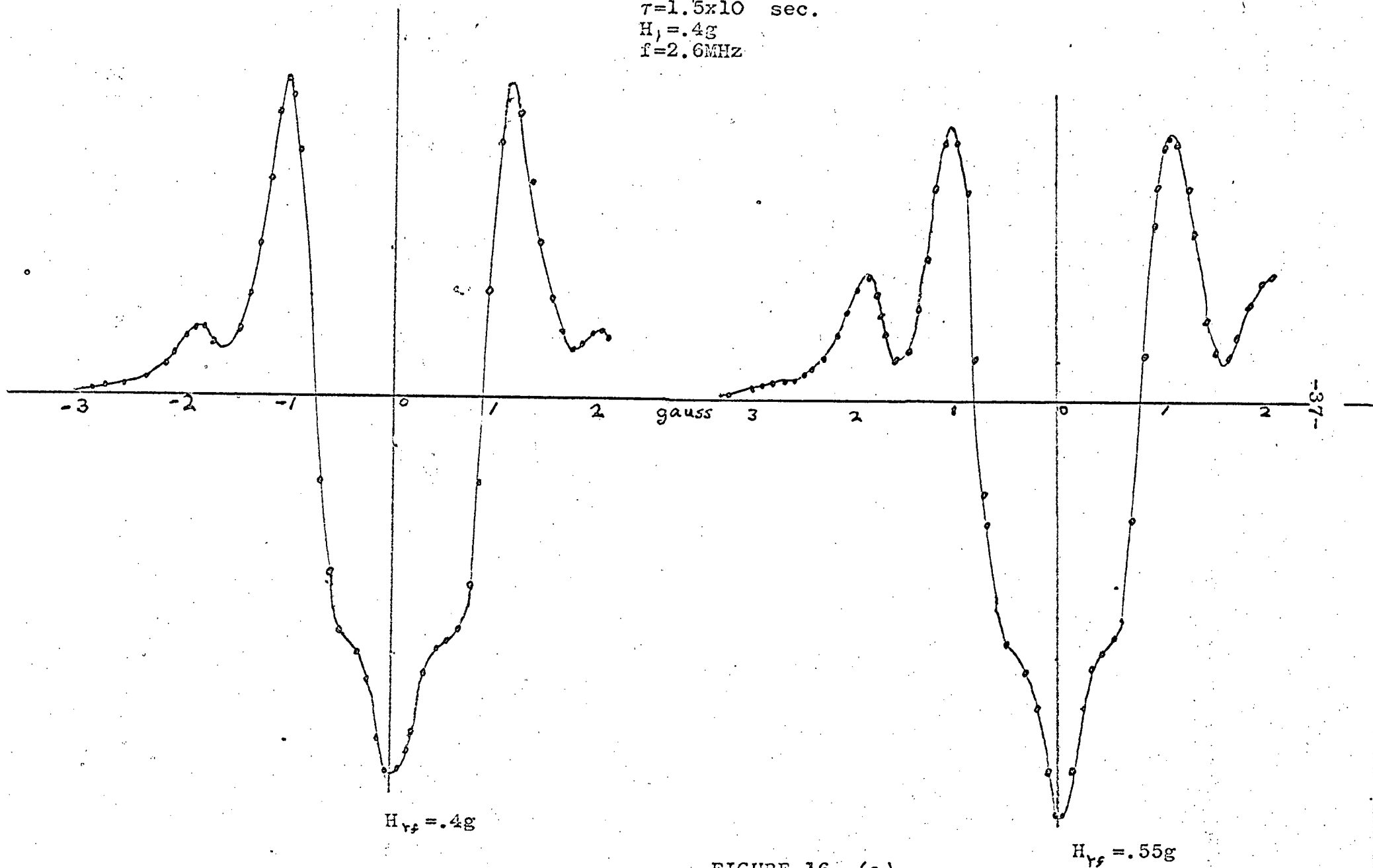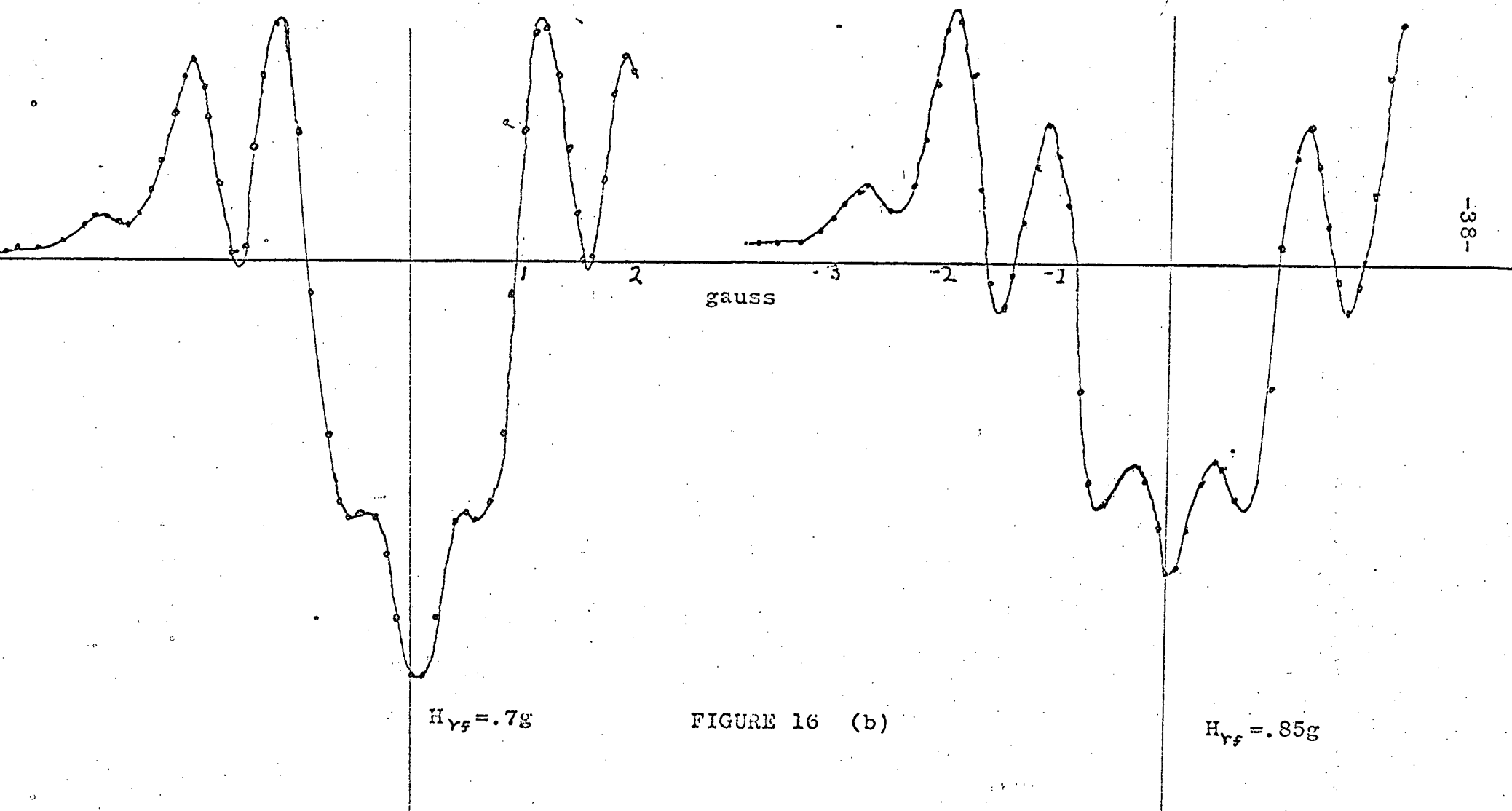
$\tau=1.5\times10^{-7}$ sec.
H$_1$ =.4g
f=2.6MHz

H$_{rf}$ =.4g

H$_{rf}$ =.55g

FIGURE 16 (a)

-38-

gauss

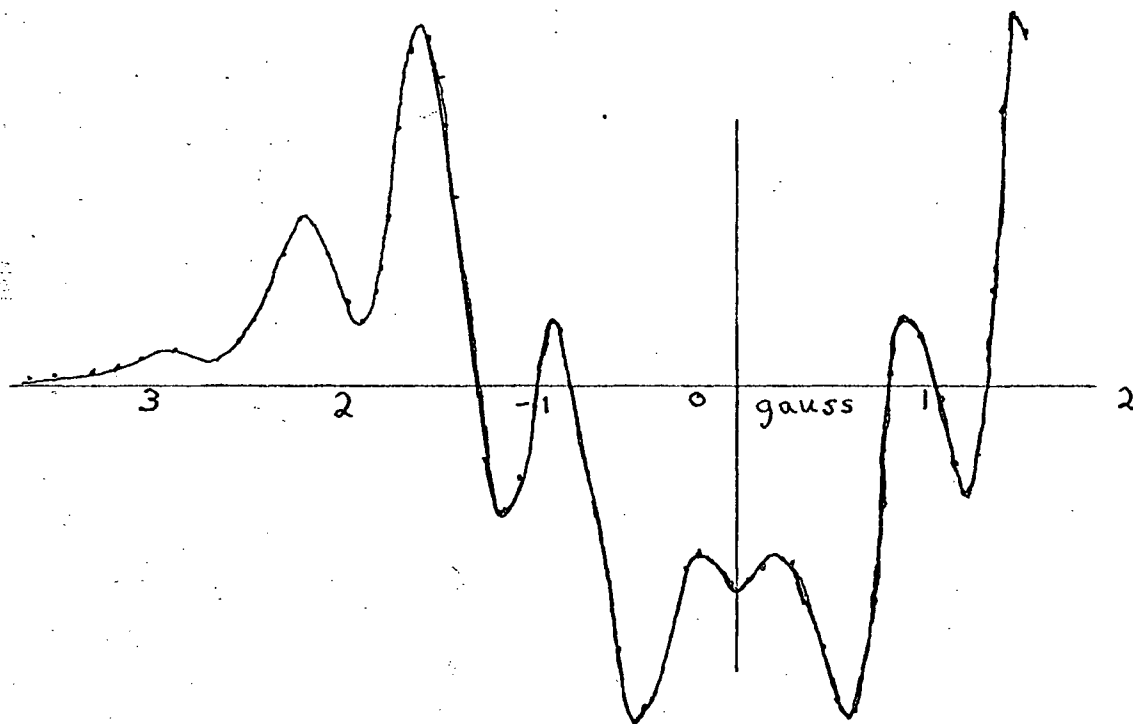$H_{rf} = .7g$ FIGURE 16   (b) $H_{rf} = .85g$

FIGURE 16   (c)   Hrf=1.0g

used for the theoretical plots are given beside the figures.
The experimental parameters agree within experimental error.
Figure 18 shows three curves which were run at approximately
the same frequency (2.6MHz) while H_1 and H_{rf} varied. Again the
experimental values agree well with the theoretical values.

A slight discrepency is that near the center of the
traces, i.e.,where $(H_o - \frac{\omega_H}{\gamma}) = 0$, the experimental curves appear
broader and show less detail than the theoretical ones. A
possible explanation is that the treatment of LiF crystals
with neutron irradiation has the effect of producing platelets
of lithium metal of about 1µ in diameter.[20] The skin depth
at 34GHz is 1 micron also. This means that the microwave
field strength could vary by 30% over the lithium particle of
1µ in diameter. If the above estimate of size is wrong and
the size is actually say .1µ in diameter, the field strength
varies by only 1 part in 10^8. Accepting the value quoted

EXPERIMENT   THEORY

(a)
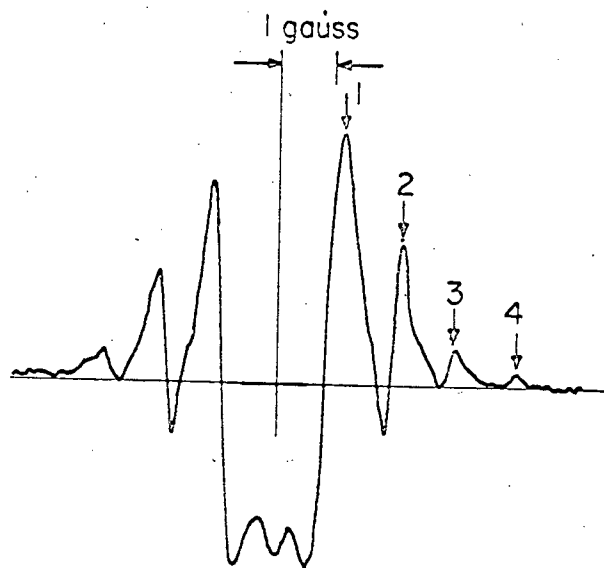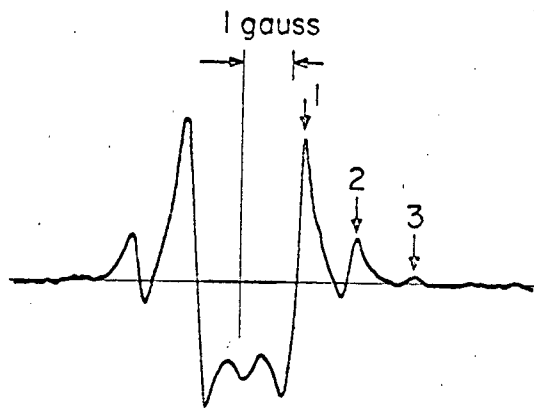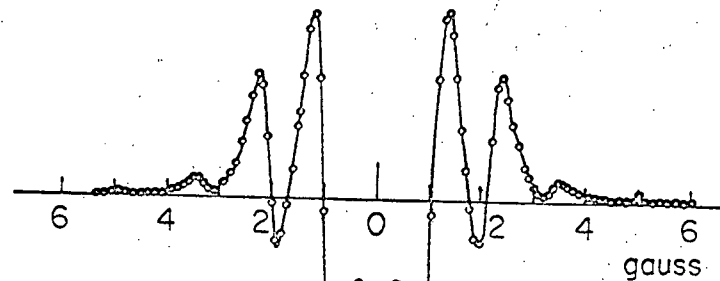
f=3.0MHz

$\tau=1.5 \times 10^{-7}$ sec.
Hrf=.9g
H =.2g

(b)
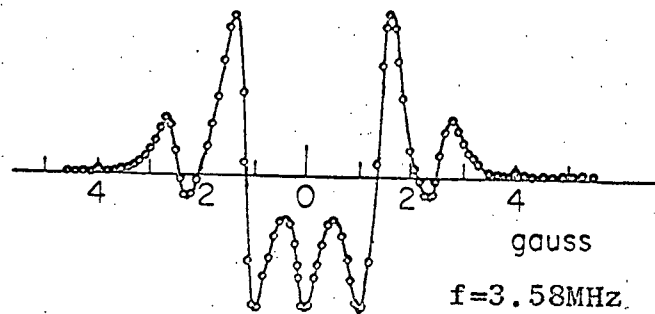
f=3.58MHz

$\tau=1.5 \times 10^{-7}$ sec.
H =.9g
H =.2g

FIGURE 17

EXPERIMENT THEORY

f=2.60MHz

$X_e=1\times10^{-6}$

$\tau=1.5\times10^{-7}$ sec.

(a)

$H_{rf}=.70g$
$H_1=.40g$

(b)

$H_{rf}=.83g$
$H_1=.60g$

(c)
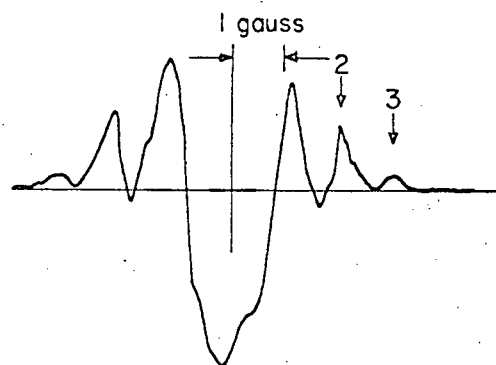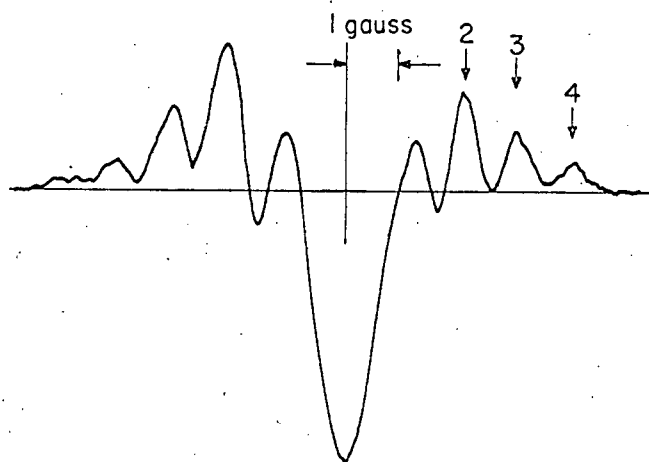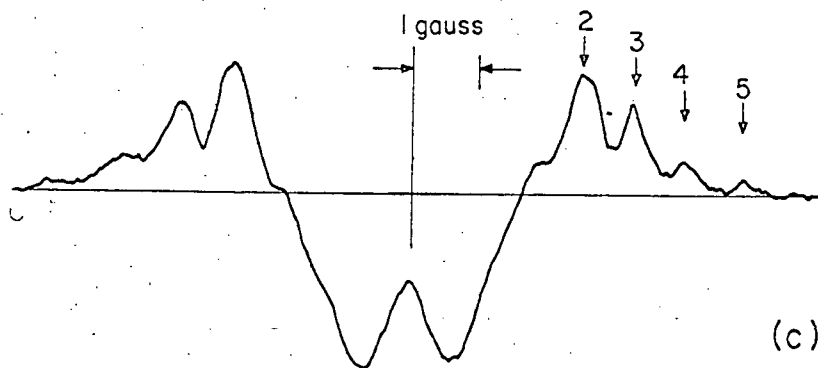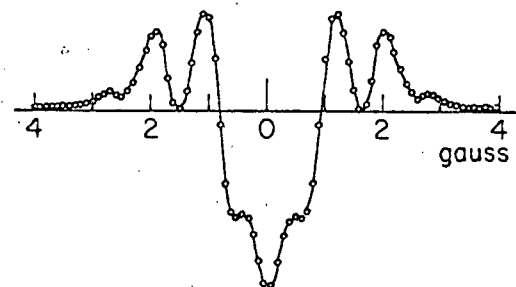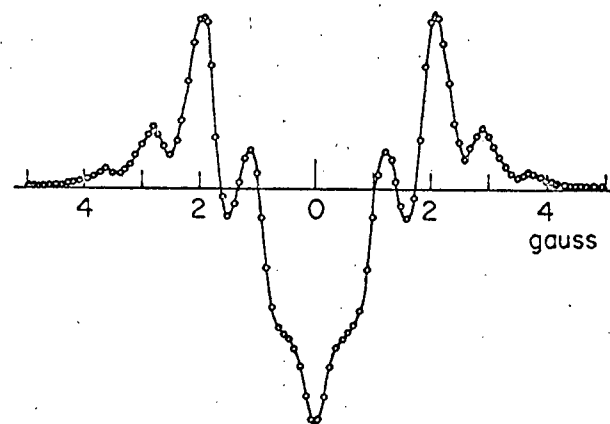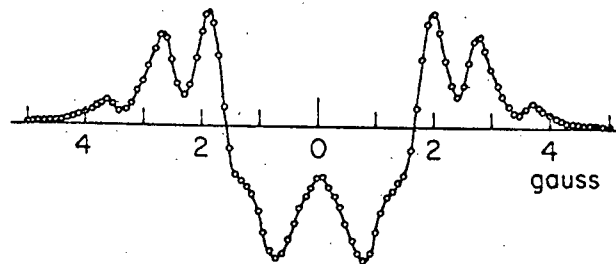
$H_{rf}=1.03g$
$H_1=.75g$

FIGURE 18

-41

above of 1μ may account for minor discrepencies of our theory
and experimental curves because near $H-\omega/\gamma=0$ a variation in H_1
causes appreciable shifting of absorption peak positions which
would for an inhomogeneous H_1 across the sample lead to a
broadening of the lines relative to those obtained by the
theory assuming a constant H_1 over the particle size.
While it is true that there should be line broadening near
the point where the klystron is resonant with the electron
Larmor frequency, $H_o-\frac{\omega}{\gamma}=0$, due to the saturation of the spin
system with the klystron power, this effect should be incor-
porated in our Bloch equation formulation and lead to no
discrepencies between the theoretical and experimental curves.

Figure 19 shows the n=1 resonance line run at about
MHz and for four values of H_1. Experimentally H_1 could not
be changed enough to observe the effect of the line shape
and peak position on H_1. This is simply accomplished with
the computer program however. At the frequency chosen H_{ess} is
about 4.5 gauss and using values of H_1 of 1,2,3,and4 gauss,
angles of up to 60 degrees can be obtained. It is noticed
that the linewidth and peak position (determined by the
derivative zero) are both strongly dependent on Θ. Figure
20 shows four curves. The curve denoted "computer" is the
peak to peak line width as a function of H_1 determined from
the computer plot. The second shows the peak to peak width
expected on the basis of a constant width in the rotating frame.
The third curve is fitted to match the second curve. Its formula
is: $Y=5/8X-.80$ where Y is the value for a point on curve

THE N=1 RESONANCE LINE RUN FOR FOUR

VALUES OF H_l H_{ess} =4.5 GAUSS

(1)   =13°

(2)   =26°

(3)   =42°

(4)   =60°

f=12.5MHz

H_{rf} =.6g

FIG. 19

-43-
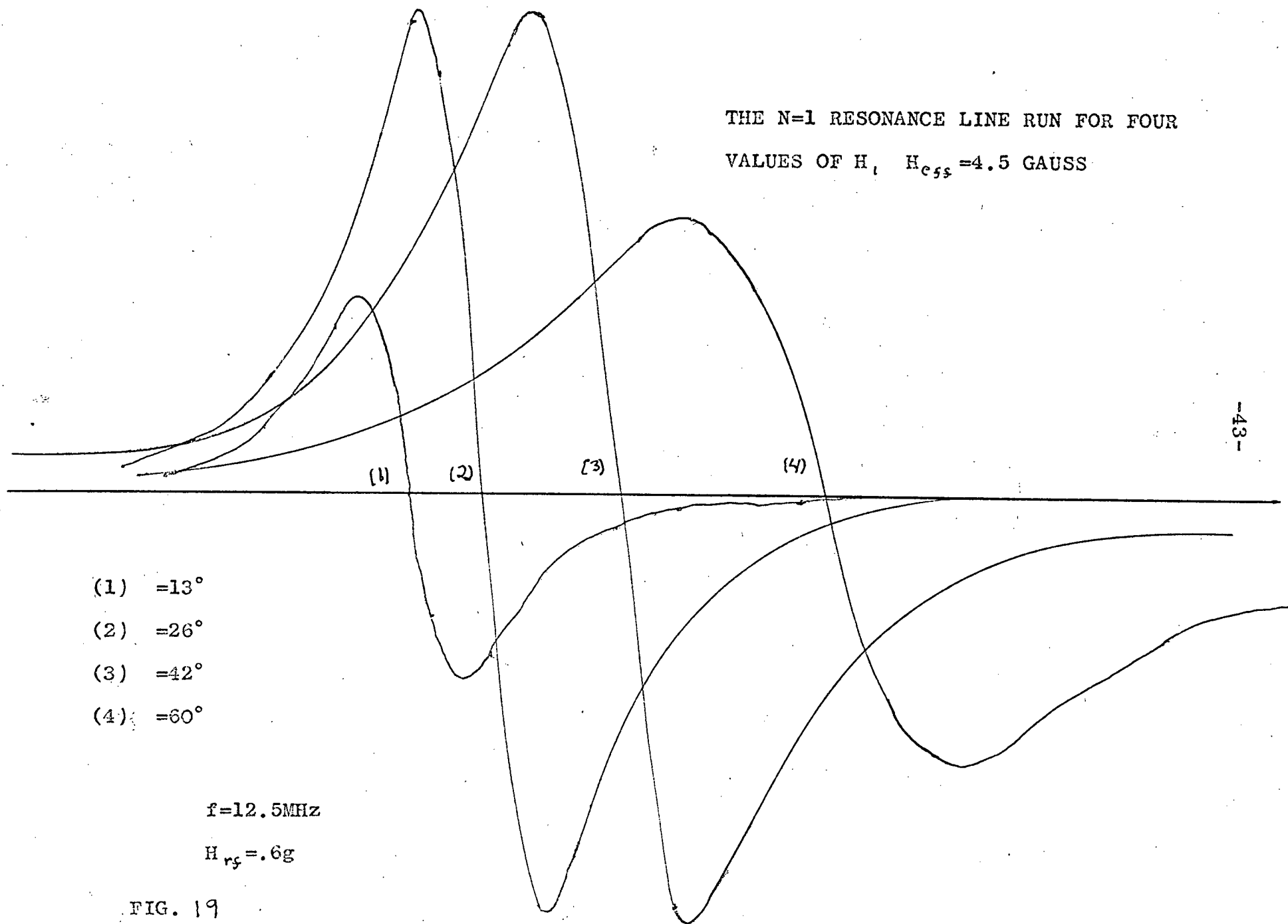
COMPARISON OF DIFFERENT PREDICTIONS OF THE LINE
WIDTH AS MEASURED IN THE LAB. FRAME

FIG. 20

Θ IN DEGREES

LINEWIDTH IN CM.

$\dfrac{A}{\cos\Theta}$

COMPUTER

$Y = \dfrac{5}{8} X - .80$

X = ORDINATE OF COMPUTER LINE

$\dfrac{(3\cos^2\Theta - 1)^2}{\cos\Theta}$

-44-
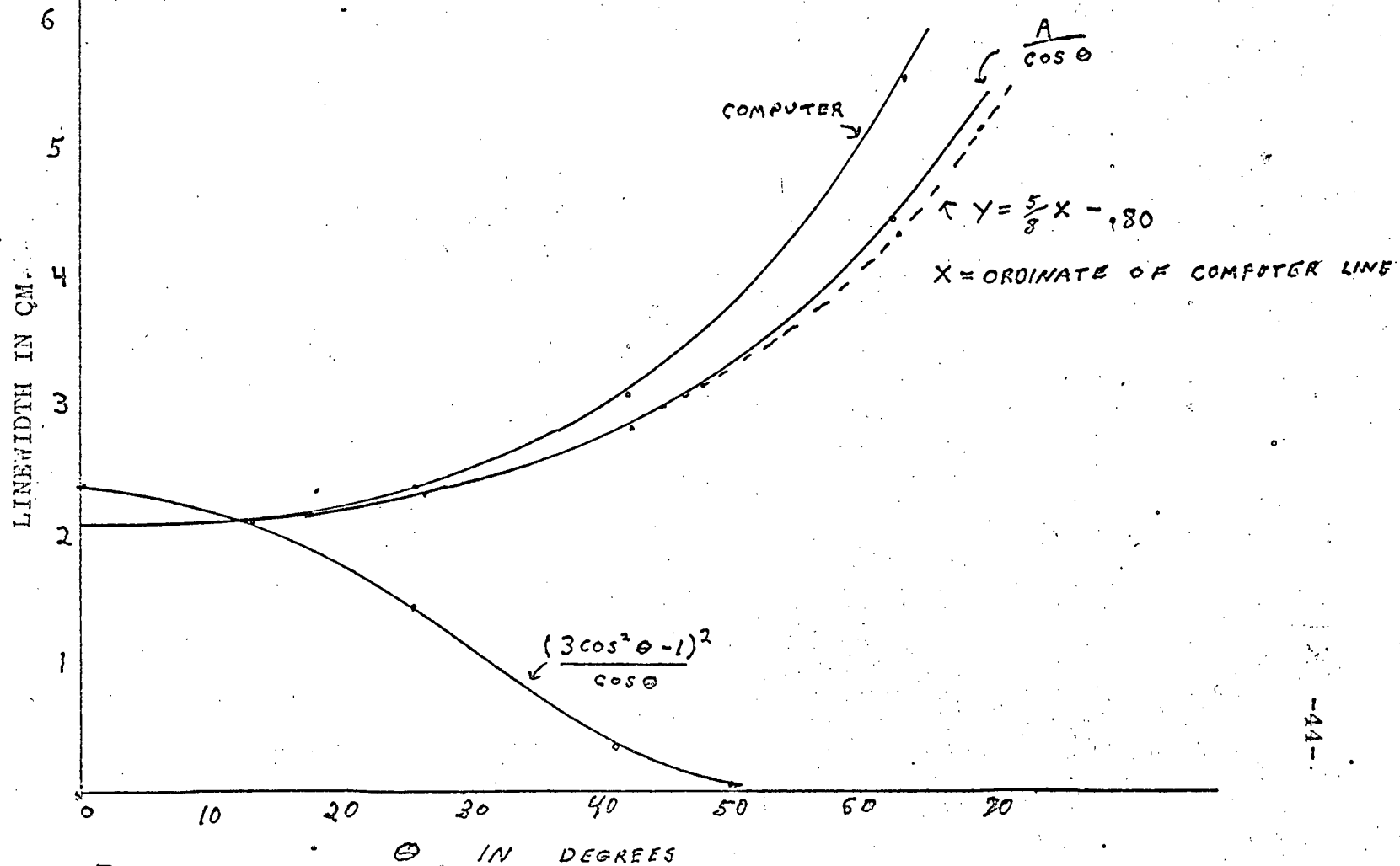
three and X is a value on curve two. The fourth curve is a plot of $\frac{(3\cos\theta-1)^2}{\cos\theta}$ which shows the dependency which one would expect if the Redfield theory were strictly applicable. While the values of H_1 used in the experiments were not large enough to completely determine this dependency, figure 9 shows that the linewidth did increase roughly as the assumption of a constant width in the rotation frame indicated it would.

From figure 1 the separation of the two n=1 resonance lines in the lab frame should be $H_{eff}\cos\theta=(H_{eff}^2-H_1^2)^{1/2}$. Since this is the formula used to obtain H_1 from the experimental results it is interesting to see if it holds for the theoretical plots. The separation is computed from figure 20 for $\cos\theta=$ .975, .895, .745, and .460 and this is compared with the separation at $\theta=0$ times $\cos\theta$. The separation of the lines on the theoretical plot does not follow $B\cos\theta$ exactly where $B=$ the separation at $\theta=0$. However for small values of θ the agreement is good and the conclusion is that equation 1.10 is a valid one to calculate H_1. Figure 21 shows this comparison.

The line separation is also affected by the Bloch Siegart effect. The expression for the position of the resonance in terms of the position where resonance would occur neglecting the effect is given by;

$$\omega = \omega_0\left(1+\left(\frac{H_{rf}}{2H_{eff}}\right)^2\right) \qquad 21$$

Taking $H_{rf}=\frac{H_{eff}}{2}$ as a typical example, $\omega = \frac{17}{16}\omega_0$. This is a shift of about 6%. The uncertainties in H_r between one run and another are greater than this so no experimental verification of the Bloch-Siegart effect was made.

SEPARATION IN THE LAB. FRAME OF THE TWO N=1 RESONANCE LINES AS A FUNCTION OF θ. (a) AS FOUND FROM THE THEORY DEVELOPED IN THE TEXT, AND (b) COSθ FOR COMPARISON

SEPARATION AT θ=0 TIMES COSθ

LINE SEPARATION IN LAB FRAME vs COSθ

SEPARATION IN GAUSS

FIG 21

COS θ

-46-
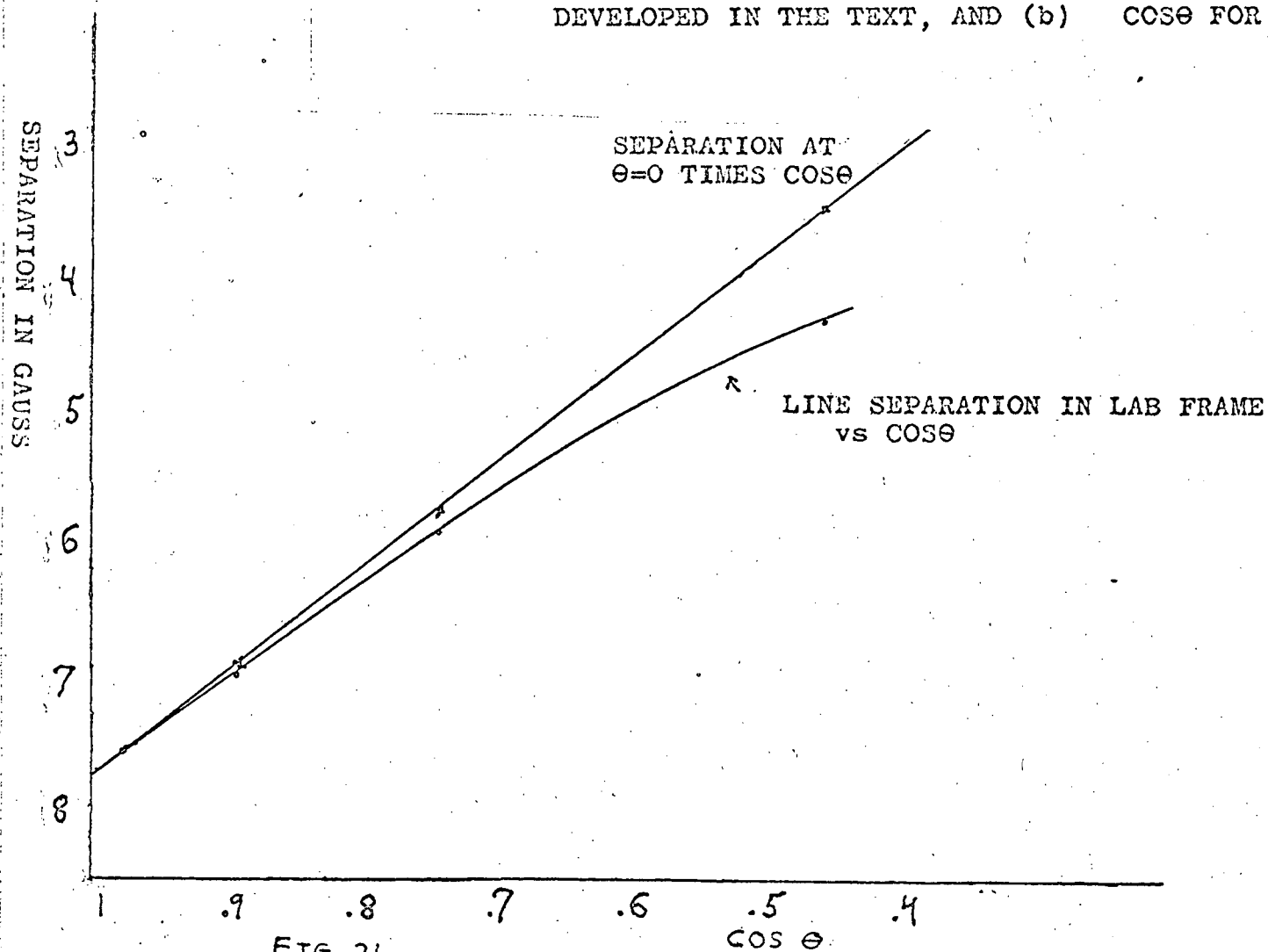
5. THE MEASUREMENT OF THE RELEVANT MAGNETIC FIELDS

It was necessary to measure and calibrate the various magnetic fields used in the experiment. The measurement of H_1 is difficult experimentally. It can be determined to some degree of accuracy from the experimental curves and the equation 1.10. However it would be desireable to make an independent direct measurement of H_1. The best way to do this is to measure the incident power to the cavity, the reflected power from the cavity and the Q of the cavity. Then knowing the field distribution in the cavity one can calculate the approximate field strength at any given point. From the definition of Q an equation relating the Q, the power dissipated in the cavity, and the magnetic field distribution in the cavity can be found. [22]

$$ Q_L = \frac{\omega}{2\pi} \frac{\int H^2 dv}{P_d} \qquad P_d = \frac{1}{Q_L} \frac{\omega}{8\pi} \int_{cavity} H \cdot H \, dv \qquad (5.1) $$

The critical measurement is thus a measure of the incident and reflected power to the cavity. These measurements were attempted with a Hewlett Packard bolometer and power measurement meter but experimental difficulties made this inaccurate. The main difficulty is that the bolometer could not be subjected to over a few milliwatts while the klystron produced about 10 watts of power. Therefore two 10db directional couplers were utilized to reduce the incident power by a factor of 10^4. The reflections from the couplings and

discontinuities in the guide system made it difficult if not impossible to determine the difference of the incident and reflected power to the cavity with sufficient accuracy. Also it was not possible to lock the klystron to the cavity and as the klystron drifts slightly from the cavity resonant frequency the field strength in the cavity can fluxuate significantly. It is for these reasons that no accurate experimental value can be given to the H_1 fields which is independent of the line separation measurements. The results of the power meter measurement was that a maximum of 1 to 2 watts of power were dissipated in the cavity. The loaded Q was measured to be 1600 and a calculation shows that the maximum field strength in the cavity is about 1.43 times the average field. These values give with our equation above a maximum H_1=3.2 gauss. This is in agreement with the values obtained by Enga but the largest H_1 fields measured in the present experiments were about one gauss. This is probably due to the fact that the sample greatly reduces the Q and most of the power is dissipated in the sample and not in the cavity. From equation 5.1 it is seen that the average field strength is proportional to the square root of Q for a given power dissipated.

A determination of the field strength H was made indirectly. In the spectrometer circuit there are two 51 K resistors which are in series and placed in parallel with the spectrometer coil. Hence the voltage across the resistors

indicates the voltage across the coil. If an attempt was
made to measure the voltage across the coil directly with
the oscilliscope the oscillator was interrupted and ceased to
oscillate. However the voltage could be measured across one
of the resistors on a fast rise time oscilliscope. The form
seemed to be a pure sine wave with very little harmonic
content over the strengths and frequencies used. Of partic-
ular interest is that the voltage varied in direct proportion
to the grid current as read on the oscillator meter. Figure
22 is a plot of the induced coil voltage vs the current read
on the oscillator meter. This data was for a 100 turn coil
operating at approximately 3.5 MHz.

FIG.   VOLTAGE ACROSS COIL IN VOLTS
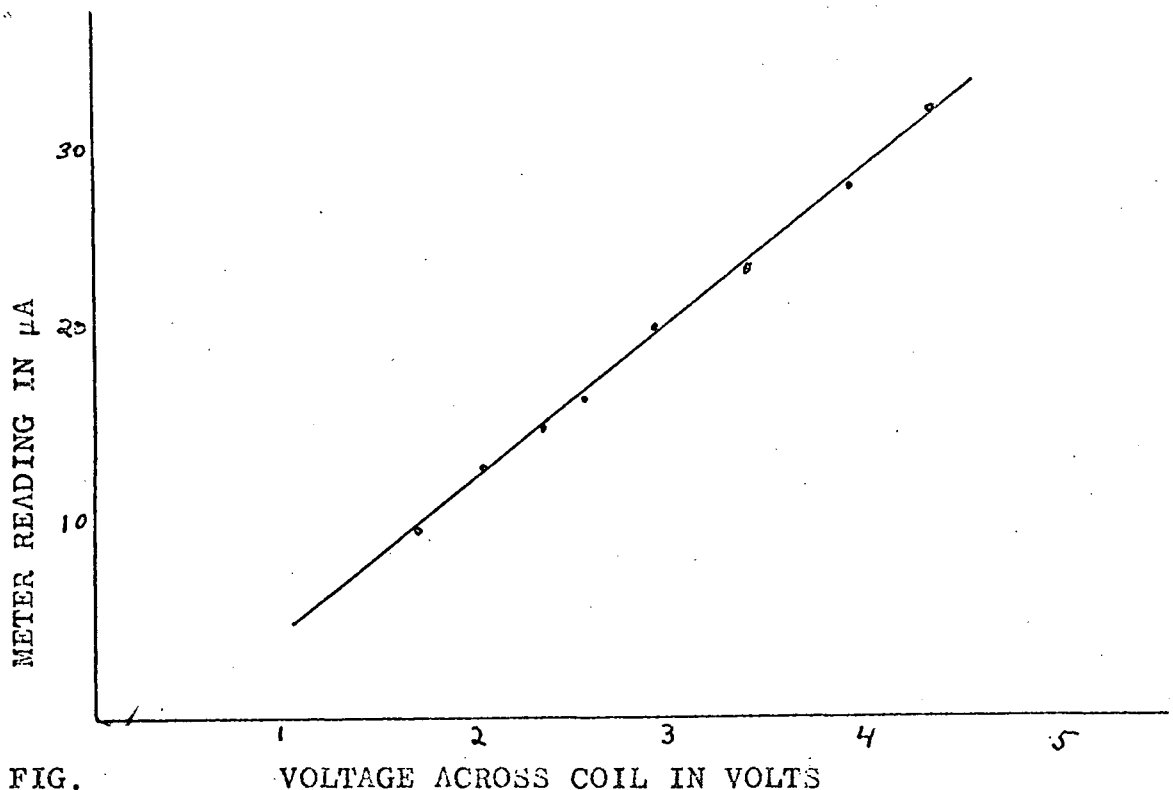
Assuming that the sample is confined to a point on the axis of the field produced by the coil and that there are negligible shielding effects due to the cavity, the field strength at the sample can be calculated knowing the voltage induced across it and the frequency of the oscillator. A sketch of the calculation follows.
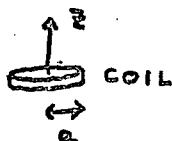
$$B_z = \frac{N \mu_0 I a^2}{2(z^2 + a^2)^{3/2}}$$

where B is in Webers per meter[2] a is in meters and I is in amps. z is the distance of the sample from the center of the coil.

$$\mathcal{E} = -L \frac{dI}{dt} \quad , \qquad I = \frac{\mathcal{E}_0 \sin \omega t}{\omega L} \quad , \qquad L = \frac{d\Phi}{dI} = \frac{N \, dB}{dI} \pi a^2$$

Solving for I

$$I = \frac{\mathcal{E}_0 \sin \omega t \; 2(z^2 + a^2)^{3/2}}{\omega N^2 \mu_0 \, a^2 \; \pi a^2}$$

$$B_z = N \mu_0 \; \frac{a^2 \left[\mathcal{E}_0 \sin \omega t \; 2(z^2 + a^2)^{3/2} \right]}{2(z^2 + a^2)^{3/2} \; \omega N^2 \mu_0 \, a^2 \; \pi a^2}$$

$$B_{z_0} \sin \omega t = \frac{\mathcal{E}_0 \sin \omega t}{\omega N \pi a^2} \qquad\qquad a \approx 2 \times 10^{-3} \, m$$

Then $\quad B_0 \approx \dfrac{\mathcal{E}_0}{f}$

Where B is in gauss E is in volts and f is in megacycles.

Using this calculation and figure 22 it is seen that for a frequency of 3.5 MHz, H_{rf} could be varied from about .4 to 1.3 gauss when the grid current reading varied from 7 to 30 μA. This corresponds closely with the experimental results as fitted by the computer program to our theory. The large magnetic field H_o was set by a field regulated power supply driving the Magnion magnet. However the field dialed in on the power supply was found to be miscalibrated by approximately 100 gauss. Also the sweep rate quoted on the power supply was found to be in error. In fact the sweep rate depended on whether the sweep was up or down. This was realized from the width of the signals. Since it was desired to know the separation of the resonances accurately the sweep had to be calibrated. The way this was done accurately was to use a separate marginal oscillator monitoring the magnetization in a glycerine sample. This oscillator was operated at about 55 MHz for the proton resonance in a 12 kilogauss field. The sweep rate could be found to three significant figures this way. At the 5 gauss per minute setting the sweep up was 3.49 gauss per minute while the rate down was 5.04 gauss per minute. Actually the rate was calibrated on the chart paper so that no errors owing to a miscalibration of the chart speed could enter.

APPENDIX

This appendix includes a complete statement of the computer program used to solve equations (2-11)-(2-29) for M_1^{ZI} and d/dt M_1^{ZI}. Below is a brief description of the symbols which appear in the program that follows. In line one M refers to the matrix of the coefficients of the magnetization. The dimension 50 is written here as it wasn't apparent in the beginning that a 36x36 would be adequate. The majority of the program is the reading in of the matrix elements. All statements of the form M(a,b) refer to specific elements. The numbers which must be supplied for the equations are: N, the dimension of the matrix, which in this case is 36, A, the maximum value of $(H_o - \frac{\omega}{\gamma})$, B, the angular frequency of the radio frequency field, C1, the spin lattice relaxation time, D, the field strength of the microwave field H_1, G, the gyromagnetic ratio of the electron, GM, the radio frequency field strength, DA, the increment in $(H_o - \frac{\omega}{\gamma})$ which was taken to be .1 gauss, Dend is the end of the sweep range of $(H_o - \frac{\omega}{\gamma})$ which was -2 gauss, GA is the electronic magnetic susceptibility of lithium which I chose to be 1×10^{-6} the Pauli paramagnetism result. Experimental evidence indicates this is low, the true value being two to three times as large.[23] However as discussed earlier this enters only as a scaling factor and hence only the relative value is of interest here. The actual solution of the matrix is carried out in a computer library subroutine. The derivative is obtained by taking

differences of M_1^{zz} for successive values of $(H_o - \frac{\omega}{\gamma})$, This
has the effect of shifting the center of the trace .05
gauss to the right. The program includes instructions to
have the output plotted, though it does not include a
scaling routine and the axes must be adjusted to fit the
particular output.

```
$TIME              10
$PAGE              50
$IBFIC MAIN
       DIMENSION M(50,50) , C(50)
       CALL PLOTS
       REAL M
       NSOS =10
       YMIN=-2.5E-3
       XMIN=-6.
       YL=10.
       XL=3.
       DY=.5E-3
       READ 10, N, A, B, Cl, D
10     FORMAT (I5, 4D15.8)
       READ 20, G, GM, DA, DEND
20     FORMAT (4E15.8)
       READ 21, GA, GAI
21     FORMAT (2E15.5)
       PRINT 101,N,A,B,Cl,D,G,GM,DA,DEND,GA,GAI
       DAD=A
101    FORMAT(I5,5E16.8/5E16.8)
       NLL=(DEND-DAD)/DA+1.5
       CALL GRID (NLL,DAD,DEND,.5,101,-20.,20.,4.)
       DO 113 II=1,5
       CALL AXIS (0.,0.,6HX AXIS,-6,XL,0.,XMIN,DX)
       CALL AXIS (0.,0.,6HY AXIS,6,YL,90.,YMIN,DY)
       A=DAD
100    DO 30 I=1,N
       DO 30 J=1,N
       M(I,J)=0.0
30     CONTINUE
       DO 40 I=1,N
       M(I,I)=1.0
40     CONTINUE
       M(7,8)=-1.0*B*Cl
       M(9,10)=M(7,8)
       M(11,12)=M(7,8)
       M(13,14)=M(7,8)*2.0
       M(15,16)=M(13,14)
       M(17,18)=M(13,14)
       M(19,20)=M(7,8)*3.0
       M(21,22)=M(19,20)
       M(23,24)=M(19,20)
       M(25,26)=M(7,8)*4.0
       M(27,28)=M(25,26)
       M(29,30)=M(25,26)
       M(31,32)=M(7,8)*4.0
       M(33,34)=M(31,32)
       M(35,36)=M(31,32)
```

```
        FACT=-1.0*G*C1*A
        NCUE=0
        NST=-1
70      DO 50 I=1,N
        NCUE=NCUE+1
        IF(NCUE.LT.3) GOTO 51
        IF(NCUE.LT.6) GOTO 50
        NCUE=0
        GOTO 50
51      J=I+2
        M(I,J)=FACT
50      CONTINUE
        IF(NST.GT.0) GOTO 60
        NST=10
        NCUE=4
        FACT=1.0*C1*G*D
        GOTO 70
60      DO 80 I=1,N
        DO 80 K=1,2
        J=I+K
80      M(J,I)=M(I,J)
        M(3,7)=2.0*C1*G*GM
        M(9,13)=M(3,7)/2.0
        M(10,14)=M(9,13)
        M(15,19)=M(9,13)
        M(16,20)=M(9,13)
        M(22,26)=M(9,13)
        M(1,9)=-1.0*M(3,7)
        M(7,15)=M(1,9)/2.0
        M(8,16)=M(7,15)
        M(13,21)=M(8,16)
        M(14,22)=M(13,21)
        M(19,27)=M(14,22)
        M(20,28)=M(19,27)
        M(7,3)=M(20,28)
        M(8,4)=M(7,3)
        M(13,9)=M(8,4)
        M(14,10)=M(13,9)
        M(19,15)=M(14,10)
        M(20,16)=M(19,15)
        M(25,21)=M(20,16)
        M(26,22)=M(25,21)
        M(9,1)=-1.0*M(26,22)
        M(10,2)=M(9,1)
        M(15,7)=M(10,2)
        M(16,8)=M(15,7)
        M(21,13)=M(16,8)
        M(22,14)=M(21,13)
        M(27,19)=M(22,14)
```

```
        M(28,20)=M(27,19)
        M(25,33)=M(7,15)
        M(26,34)=M(25,33)
        M(31,27)=M(26,34)
        M(32,28)=M(31,27)
        M(27,31)=-1.0*M(32,28)
        M(28,32)=M(27,31)
        M(33,25)=M(28,32)
        M(34,26)=M(33,25)
        DO 90 I=1,N
90      C(I)=0.0
        C(2)=GAI*D
        C(5)=1.2E-2
        C(6)=GAI*A
        C(11)=GA*GM
        IF(NSOS.GT.0) GO TO 200
        NSOS=10
        CALL MATOUT (M,N,50)
        CALL VECOUT (C,N)
200     CONTINUE
        CALL SOLTN(M,C,N,50,DET)
        CC=(C(12)-CC)*10.
        PRINT 78,A,C(12),CC,DET
78      FORMAT (1P4E16.6)
        CALL POINT (A,CC*1.E+4,II)
        XX=(A-XMIN)/DX
        YY=(CC-YMIN)/DY
        CALL SYMBOL (XX,YY,.07,3,0.,-1)
        CC=C(12)
        A=A+DA
        IF (A.GT.DEND) GO TO 112
        GO TO 100
112     D=D+.25
        CALL PLOT (1.5*XL,0.,-3)
113     CONTINUE
        CALL PLOTND
        CALL OUTPUT
99      STOP
        END
```

BIBLIOGRAPHY

1.   Pake, G., Paramagnetic Resonance W.A. Benjamin Inc. New York. 1962

2.   Redfield, A., Phys. Rev. 98, 1787 (1955)

3.   Franz, J., Doctoral Thesis, U. of Illinois, 1965 (unpublished)

4-5. Abragam, A., The Principles of Nuclear Magnetism (Oxford University Press. London, 1961)

6-7. Redfield, A., Phys. Rev. 98, 1787 (1955)

8.   Enga, E., Masters Thesis, U.B.C., 1966 (unpublished)

9.   Ryter, Ch., Phys. Rev. Letters, 5, 10, (1960)

10. Garstens, M.A. and Kaplan, J.I., Phys. Rev. 99, 459 (1955)

11. Whitfield, G., and Redfield, A.G., Phys. Rev. 106, 918 (1957)

12. Koss, T.A., Alexander, S., and Schwerdtfeger, C.F. Can. J. Phys. (August 1968)

13. Enga, E., op. cit.

14. Benedek, G.B. and Kushida, T., Phys. Rev. 118, 46 (1960)

15. Volkoff, G., Petch, H., and Smellie, D., Can. J. Phys. 30, 270 (1952)

16-17. Winter, J.M., Ann. de Phys. 4, 745 (1959)

18. Schwerdtfeger, C.F. and Koss, T.A., Phys. Rev. 166, 259 (1968)

19. Abragam, A., op. cit.

20. Ryter, Ch., op. cit.

21. Abragam A., op. cit.

22. Portis, A.M., Phys. Rev. 91, 1071 (1953)

23. Schumacher, R.T. and Slichter, C., Phys. Rev. 101, 58 (1956)